ANL-7101

Argonne National Laboratory

ELASTICITY AND ANELASTICITY OF URANIUM OXIDES AT ROOM TEMPERATURE

by

Roberto J. Forlano, Alfred W. Allen,
and Robert J, Beals

LEGAL NOTICE

Printed in USA. Price $3.00 . Available from the Clearinghouse for Federal Scientific and Technical Information, National Bureau of Standards, U. S. Department of Commerce, Springfield, Virginia 22151

ANL-7101
Metals, Ceramics, and
Materials (TID-4500)
AEC Research and
Development Report

ARGONNE NATIONAL LABORATORY
9700 South Cass Avenue
Argonne, Illinois 60439

ELASTICITY AND ANELASTICITY OF URANIUM OXIDES AT ROOM TEMPERATURE

by

Roberto J. Forlano, Argonne National Laboratory and
The University of Illinois
Alfred W. Allen, The University of Illinois
Robert J. Beals, Argonne National Laboratory

Metallurgy Division

Metallurgy Program 9.5.14

Portions of the material in this report have appeared in the following Metallurgy Division Annual Report:

Report No.	Pages	Date
ANL-7000	99-101	1964

December 1965

Operated by The University of Chicago
under
Contract W-31-109-eng-38
with the
U. S. Atomic Energy Commission

FOREWORD

The present report is based on a thesis submitted by Roberto J. Forlano in partial fulfillment of the requirements for the degree of Doctor of Philosophy in Ceramic Engineering, University of Illinois, Urbana. This research was supervised by Alfred W. Allen, Professor of Ceramic Engineering, University of Illinois, and Dr. Robert J. Beals, Associate Ceramic Engineer, Argonne National Laboratory.

TABLE OF CONTENTS

TABLE OF CONTENTS

LIST OF FIGURES

LIST OF FIGURES

LIST OF TABLES

ELASTICITY AND ANELASTICITY OF URANIUM OXIDES AT ROOM TEMPERATURE

by

Roberto J. Forlano, Alfred W. Allen,
and Robert J. Beals

I. INTRODUCTION

The theory of elasticity is based on the assumption that stress and strain are directly related. This is an oversimplification. The fact that these parameters are not in phase is taken into consideration in the study of anelasticity, which makes this type of investigation a desirable complement for elastic studies. Anelasticity not only permits the elucidation of basic problems such as internal structure or atomic motion, but also can be used to determine the damping capacity of the material.

Mechanical properties of a solid are closely related to microstructure.[1] It is difficult to draw plausible conclusions of elastic and anelastic behavior without a full knowledge of the microstructure. Elastic modulus is affected, for example, by porosity and the presence of a second phase. Grain boundaries, crystalline inversions, dislocation density, porosity, and stoichiometry have been shown to affect the anelastic properties of a solid.[2]

Uranium oxide was chosen as the material for the present investigation because of its importance in the field of nuclear ceramics, the scarcity of elastic and anelastic data, and the complexity of the system. Uranium oxide is used as a fuel element because of such good characteristics as high melting point, large uranium concentration, stability to irradiation, and ease of fabrication and reprocessing. Considerable research has been performed on this solid; however, Belle,[3] in his excellent summary of the properties of UO_2, listed only five references related to the elastic traits and none with respect to anelasticity. The complex uranium-oxygen system with solid solution and two phase regions is an ideal material for a research project with emphasis on the microstructural viewpoint.

This work was undertaken to provide information on the elastic and anelastic behavior of uranium oxide at room temperature, relating it to such microstructural aspects as number, size, shape, and position of the pores; grain size; and the number and types of phases present.

II. LITERATURE SURVEY

A. Theoretical Considerations

The elastic moduli can be determined by static or dynamic techniques. Static tests are advisable for determining the effect of stresses, but present the disadvantage that at elevated temperature, creep will render the results inaccurate. In the dynamic method, the elastic modulus is usually determined at a very small stress level, and the results are very sensitive to changes in the material. Another inherent advantage is that this method also permits the determination of anelastic effects. Dynamic tests can be divided into the resonant-frequency type and the wave-velocity type. In the first type, vibrations are excited in the sample by mechanical or electronic means, and the resonant frequency is found by determining the maximum amplitude of vibration. Young's modulus can be computed from the flexural or longitudinal resonant frequencies, and the shear modulus from the torsional resonant frequency. Pickett[4] expressed Young's modulus by the equation

$$E = CWf_r^2, \tag{1}$$

where E is Young's modulus, W is the weight of the specimen, f_r is the flexural resonant frequency, and C is a factor that depends on the shape and size of the specimen, the mode of vibration, and Poisson's ratio. The value of C can be obtained for cylinders and prisms from graphs presented by Pickett.[4] Spinner et al.[5] developed empirical relations by which Young's modulus may be determined from the longitudinal and flexural resonant frequencies. They stated that Pickett's equation gives too high a value for the correction factor of cylindrical specimens. The results obtained apply mainly to those materials having Poisson's ratio of approximately 0.3. Spinner and Tefft[6] and Lakin[7] explained thoroughly how to excite and detect the different types of vibration and also gave the different equations and tables needed for the calculation of Young's and shear modulus. Hasselman[8] published tables that simplified the calculation of the elastic modulus for a wide range of Poisson's ratio and dimensions. Spinner and Valore[9] determined empirical curves to be used to find the shear modulus of bars of rectangular cross section from their resonant frequencies. Tefft and Spinner[10] developed relations to compute the shear modulus of bars having square cross sections.

In the wave-velocity method, a wave in the sonic or ultrasonic range is transmitted in the solid to be studied. Three groups of waves are formed: longitudinal, transverse, and Rayleigh or surface waves. The longitudinal or compressional waves permit the calculation of Young's modulus, and the transverse or shear waves are used to determine the shear modulus. This technique is discussed in detail by Mason[11] and Kolsky.[12]

The sonic technique, as mentioned before, is suitable for the determination of the anelasticity of solids. The subject is treated completely by Zener.[13]

If stress (S) were solely related to strain (ϵ), the relationship between them would be

$$M\epsilon = S, \tag{2}$$

where M is the elastic modulus. Experimental observations have demonstrated that this assumption is too simplified. The term anelasticity is used to express a more exact time-dependent relationship between stress and strain. There are different manifestations of anelasticity. For example, one is the occurrence of elastic after-effects consisting of residual deformation that gradually disappears when the stress is removed. Another case is internal friction or damping, represented by the symbol Q^{-1}, which consists of the dissipation of vibrational energy. An equation to replace the relation expressed in Equation (2) that fits the experimental data is

$$a_1 S + a_2 \frac{dS}{dt} = b_1 \epsilon + b_2 \frac{d\epsilon}{dt}, \tag{3}$$

where a_1, a_2, b_1, and b_2 are constants; S is the stress; dS/dt is the stress rate; ϵ is the strain; and $d\epsilon/dt$ is the strain rate.

By appropriate manipulations of (3),

$$M_U = M_R \frac{\tau_s}{\tau_\epsilon}, \tag{4}$$

where M_U, equal to $\Delta S/\Delta\epsilon$, is the unrelaxed modulus; M_R is the relaxed modulus; τ_s is the time of relaxation of strain under constant stress; and τ_ϵ is the time of relaxation of stress at constant strain.

When stress and strain are sine functions of time,

$$M_\omega = M_U - \frac{M_U - M_R}{1 + (\omega\overline{\tau})^2} \tag{5}$$

where M_ω is the ratio of the stress to the portion of the strain that is in phase with the stress; ω is the angular frequency of the oscillation; and $\overline{\tau}$ is equal to $(\tau_s \tau_\epsilon)^{1/2}$.

In the limit,

$M_\omega = M_U$, when $\omega\overline{\tau} \gg 1$;

$M_\omega = M_R$, when $\omega\overline{\tau} \ll 1$.

This explains the difference in the elastic modulus measured by different methods. When the elastic modulus is determined by a dynamic technique, the unrelaxed modulus (M_U) is measured; when the static method is used, the relaxed modulus (M_R) is obtained.

The most popular methods of determining the internal friction are: (1) measuring the half-width of the resonant peak at forced vibrations, and (2) estimating the decay of the vibrations in the free sample. Zener[13] has shown that in the first case the damping is given by

$$Q^{-1} = \frac{\Delta f}{f_r \sqrt{3}}, \tag{6}$$

where Δf is the width of the resonant peak at half the maximum amplitude, and f_r is the resonant frequency. In the second case, the internal friction is estimated from

$$Q^{-1} = \frac{\ell n (A_0/A_n)}{\pi f_r \Delta t}, \tag{7}$$

where A_0 is the amplitude of vibration when the excitation is stopped, A_n is the amplitude of vibration after a time Δt, f_r is the resonant frequency, and Δt is the time between amplitudes A_0 and A_n.

These two methods supplement each other. When the internal friction is very low, the half-width becomes very small and is difficult to determine; hence, it is advisable to use the decay method. When the damping is large, the attenuation is extremely fast, making the determination of Δt cumbersome; therefore, in this case, the half-width method is recommended.

B. Instrumentation

Many devices are used for determining the elastic modulus and internal friction of solids. Table I indicates methods used in the 1-100,000-cps frequency range. Mason[11] and Kolsky[12] gave a good account of the equipment used in the ultrasonic region. This frequency range has been used in the study of glass and quartz.[25-30] Little work has been done in ceramic materials at ultrasonic frequencies, mainly because of the problems encountered at elevated temperature in coupling transducers to specimens and in the interpretation of data. This technique deserves more consideration, and attention should be given to the possibility of using the momentary-contact method described by Carnevale et al.[31]

TABLE I. Techniques for Determining Elastic Modulus and Internal Friction in 1-100,000-cps Frequency Range

Technique	Advantages	Disadvantages	Key References
Pendulum	Good for very high values of internal friction, and high temperature.	High damping background. Samples difficult to fabricate.	14, 15
Mechanical	Simple. Very high driving force.	Lack of accuracy. High damping background.	16
Piezoelectric	Small damping background.	Temperature range is limited (~600°C). Small driving force.	17, 18, 19
Electrostatic	Very small damping background.	Temperature range is limited (~1000°C). Very small driving force. Electrode gap changes.	20, 21, 22, 23
Electromechanical	Good for high temperature. Large driving force.	Stray vibrations from coupling wires. Measurements are affected by position of support.	24

For studies of metals and glasses, the most popular method is that of the torsion pendulum.[32-34] The apparatus consists basically of a pendulum bob and a supporting member; the specimen is usually 0.02 to 0.1 cm in diameter. The frequency range used is 0.5 to 5 cps. Kofstad et al.[35] by employing electromechanical principles, extended the frequency range to about 50 to 500 cps. Chang[36] and Dew[14] utilized apparatus based on the same concept for the study of relaxation processes in ceramics. The main problem with their method is the difficulty in fabricating ceramic specimens of proper size and shape. The high background damping makes this technique unsuitable for determining small values of internal friction, but lends itself well to the study of phenomena with high damping peaks as, for example, grain-boundary relaxation.

Different types of excitation can be used in the resonant-frequency technique. Ault and Ueltz[16] used a mechanical form of excitation by striking the test bar with a long rod. Balamuth,[17] Read,[18] and Marx[19] used a piezoelectric method of excitation. A properly cut quartz crystal is cemented to the specimen. The driving force is produced by the change in the dimensions of the crystal when an electrical signal is applied. The main drawback of this method, at elevated temperature, arises from the cementing of the specimen to the crystal, each having different coefficients of thermal expansion. Fraser and LeCraw[37] developed an ingenious technique for measuring the internal friction, elastic constants, and Poisson's ratio. The specimen consisted of a small sphere placed on a shear mode transducer, which was driven with a pulse at one of the resonant frequencies of the sphere. The free decay of the amplitude of vibration of the sphere was detected by switching the transducer to a receiver. This method permitted values of Q^{-1} as low as 3×10^{-7} to be measured. The method was used up to 400°K.

In the electrostatic method, the vibrations are produced by a capacitor formed by one end of the specimen and a plate, fixed very close to the same end. Another similar capacitor at the other end determines the amplitude of vibration. This method was developed by Bancroft and Jacobs[20] and adapted to measurements up to 500°C by Dickson and Strauch.[21] Improvement in the apparatus allowed measurements up to 700°C; this limit was set by the weakness of the signal due to the attenuation in the sample.[22] Sneed et al.[23] studied metals up to about 1000°C and claimed that with changes the instrument could work at higher temperatures. Inconveniences of this method are: (1) a conducting coating must be applied to nonconducting specimens, (2) the maximum temperature attainable is rather low, (3) the gap between the plates of the capacitor has to be adjusted because of the expansion of the sample, and (4) a large driving voltage is necessary because of the weakness of the signal. This method is recommended for measuring very small values of internal friction because the damping in the instrument itself is quite low.

The electromechanical method of excitation and detection was pioneered by Förster.[24] A simple device such as a recording cutting head or a speaker is generally used to excite the specimen. The amplitude of vibration is picked up with another transducer. If the test is performed at elevated temperature, the coupling usually is made through threads or wires. Roberts and Nortcliffe[38] claimed that cotton threads were the most suitable means of coupling at room temperature, because they did not introduce stray vibrations. At temperatures up to 1000°C, asbestos strings were used by the above-mentioned workers,[38] and fiberfrax yarns by Baskin et al.[39] Wachtman and Maxwell[40] used asbestos to about 1200°C, although they found that at about 600°C the material began to lose its flexibility and produced erratic vibrations. They recommended platinum wire, no larger than 10 mils in diameter for tests performed in air in the range of 600-1300°C. When the studies were made in vacuum, they used molybdenum wires (2 to 5 mils) up to 1700°C. Brown and Armstrong[41] excited longitudinal vibrations with tungsten wires in vacuum at 2000°C. Threads of an inorganic material* were employed in tests performed up to 1600°C in vacuum.[42] The coupling, when the excitation source is a speaker, can also be performed through air.[43] Willmore et al.[44] used nickel rods for exciting the specimen and detecting the signal. They mentioned that the pressure of the pickup should be adjusted according to the instructions of the manufacturer to obtain best results. This system, although working very well in the determination of Young's modulus, presents the problem of high damping in the instrument, reducing the sensitivity for internal friction measurements. Wachtman et al.[45] used fine phosphor-bronze springs to facilitate the detection of the torsional resonance frequency.

The electromechanical method is suitable for studies at elevated temperatures. Theoretically, the limitation in the temperature would be

*"Pluton," manufactured by Minnesota Mining and Manufacturing Company.

imposed solely by the furnace, because the transducers can be placed at any distance from the heating zone. However, the coupling usually presents problems. Refractory metal wires have their own resonant frequency, which can be mistaken for those corresponding to the sample. Another factor to be considered is that the position of the supports affects the internal-friction results.[46]

Many workers have refined the technique for detecting the amplitude of vibration and determining the damping. The low-frequency vibrations from the floor or bench have been minimized by connecting a small capacitor in series with the output leads of the pickup.[38] For measuring the internal friction by the decay method, Förster and Breitfeld[47] used an electronic device for counting the number of cycles between two determined amplitudes of vibration. Marlowe and Wilder[42] accomplished the same thing by photographing the oscilloscope trace of the damped-sine-wave signal. Wachtman and Tefft[46] used a storage oscilloscope to record the decay. An electronic circuit for very accurate measurements of the internal friction is described by Pattison.[48] Thompson and Holmes[49] and Brown et al.[50] employed an oscillator sweep and an X-Y recorder to trace the resonance curve, and the half-width of the peak was measured from the graph. The same system was used for hot-cell application.[51] Sosin et al.[52] described a technique in which the changes in internal friction were determined by measuring the driving force necessary to maintain the amplitude of vibration constant at the resonant frequency. Harlow et al.[53] explained a frequency-modulation method using standard electronic equipment for measuring internal friction. Brown and Armstrong[41] eliminated low-frequency, mechanical vibrations by increasing the resistive load in the pickup and using a band-pass filter following the preamplifier. Detwiler and Holden[54] used a travelling microscope for measuring the difference of amplitude between a determined number of cycles. Smith and Berns[55] described another method in which the damping was determined as a function of the frequency and phase changes.

Elastic modulus and internal friction can be determined dynamically with a large variety of apparatus, ranging from standard electronic equipment in which the measurements are performed manually, to elaborate electronic circuits for recording the results automatically. The choice depends on the maximum temperature of the tests, the magnitude of the internal-friction values expected, the mode of elastic response to be measured, and the specific elastic moduli to be studied.

C. Elastic Modulus and Internal Friction of UO_2

The results found in the literature on the elastic properties of UO_2 have been grouped in Table II. Lambertson and Handwerk,[56] while studying the fabrication and physical properties of urania bodies, obtained a Young's modulus of 1450 kilobars.* This was calculated by measuring the deflection

*1 kilobar = 10^9 dynes/cm^2 = 1.4504 x 10^4 lb/in.^{2} = 2.0886 x 10^6 x lb/ft^2 = 1.01971 x 10^6 g/cm^2 = 10.1971 x 10^6 kg/m^2.

TABLE II. Elastic Modulus of UO_2

Reference	Starting Powder	Binder	Density, gm/cc	Volume Fraction Porosity	Average Grain Size Micron	O/U	Technique	Test Temperature, °C	Young's Modulus, kilobars	Shear Modulus, kilobars	Poisson's Ratio
Lambertson and Handwerk[56]	MCW[a]	-	10.6	0.0329	-	-	Static	25	1450	-	-
Bowers et al.[57]	MCW[a]	Yes	9.52	0.1314	25	-	Dynamic	25	1524	-	-
	MCW[a]	Yes	10.12	0.0767	25	-	Dynamic	25	1468	-	-
Johnson[58]	-	-	-	-	-	-	-	25	1725	-	-
Belle and Lustman[59]	From Ammonia Precipitated Diuranate	-	10.20	0.0694	-	-	Dynamic	25	1820	-	-
								100	1795	-	-
								200	1762	-	-
								300	1737	-	-
								400	1715	-	-
								500	1700	-	-
								600	1685	-	-
								700	1665	-	-
								800	1635	-	-
Scott et al.[60]	(b)	no	10.5	0.0420	2 to 10	2.16	Dynamic	25	1240	-	-
	(c)	no	10.3	0.0613	2 to 10	2.00	Dynamic	25	1860	-	-
Wachtman et al.[61]	-	-	10.38	0.0530	-	-	Dynamic	25	1935	-	-
								200	1888	-	-
								400	1848	-	-
								600	1809	-	-
								800	1767	-	-
								1000	1724	-	-
								1100	1696	-	-
Lang[62]	MCW[a]	-	10.37	0.0539	-	2.02	Dynamic	25	1829[d]	741	0.302[e]
	Ammonia Precipitated	-	10.19	0.0703	-	-	Dynamic	25	1823[d]	706	0.29[e]
Wachtman et al.[63][c]	(f)	-	-	-	-	2.00	Ultrasonic	25	2305[g]	875[g]	0.317[e,d]

[a] Mallinckrodt Chemical Works.

[b] Prepared from nonstoichiometric powder.

[c] Obtained from the nonstoichiometric specimen by reduction in hydrogen at 1200°C for 2 hours.

[d] Calculated from the longitudinal resonant frequency.

[e] Calculated from the expression: $\mu = \frac{E}{2G} - 1$.

[f] The sample was a single crystal.

[g] Calculated from the mean of the Voight and Reuss average.

of a rod with a density of 10.6 g/cm^3 and a modulus of rupture of 1750 kg/cm^2. Bowers et al.[57] determined Young's modulus by a sonic method on specimens approximately 1.27 cm in diameter and 12.70 cm long. The specimens were prepared by pressing isostatically at 7000 kg/cm^2 and sintering at 1750°C for 2 hr in hydrogen. They reported a larger value for the specimen having the lower density. This is unusual because the elastic modulus normally increases with density. No explanation was given for this behavior. These authors[57] determined the elastic modulus of uranium oxide with additives. Silica, zirconia, and ceria reduced the elastic modulus, while beryllia increased it slightly. Minor additions of titania or ceria improved the sintering characteristics of UO_2-BeO bodies, but no information was given about the elastic properties of the specimens. Johnson[58] reported data on the elastic modulus of UO_2, but the characteristics of the specimens or of the method employed in the measurements are not mentioned. Belle and Lustman,[59] in describing the properties of uranium oxide, reported values of Young's modulus over the range of 25 to 825°C. The modulus of elasticity decreased with temperature (10%) in a nonlinear form. An inflection point was noted at about 300°C, suggesting the probability of a relaxation phenomenon at this temperature. Scott and co-workers[60] observed that Young's modulus decreased markedly as the oxygen-to-uranium atomic ratio of the specimen increased. The test bar was prepared by isostatically pressing nonstoichiometric powder and sintering at 1450°C in nitrogen. The stoichiometric specimen was obtained by reducing the sample mentioned above in hydrogen at 1200°C for 2 hr. Scott et al.[60] claimed that this procedure did not affect the porosity or the grain size; however, they did not report the phases present in the nonstoichiometric rod, and no information is given about the microstructural homogeneity before or after the reducing treatment. Wachtman et al.,[61] while studying the elastic properties and internal friction of several refractory oxide materials, measured Young's modulus of UO_2 as a function of temperature. The elastic modulus decreased by 11% from room temperature to 1000°C. The change was nonlinear, and an inflection point was observed at 300°C. An internal friction value of 4.3×10^{-5} was reported at room temperature. There is no indication whether this measurement was performed in air or in vacuum. Lang,[62] during the course of a study covering the properties of ceramics and cermets, determined the elastic properties of uranium oxide. The difference between the data obtained in two different groups of samples (see Table II), may be attributed to such factors as starting material, density, microstructure, or stoichiometry. No attempt was made to analyze these possibilities. The most recent information on the elastic properties of UO_2 has been reported by Wachtman et al.[63] The elastic constants of a single crystal of UO_2 at 25°C were: C_{11} = 3950 kilobars, C_{12} = 1210 kilobars, and C_{44} = 641 kilobars. The determination was performed by velocity measurement at 10 Mc/sec with the use of X-cut and AC-cut quartz crystals 6.5 mm in diameter to generate the longitudinal and transverse waves, respectively. A maximum value of 3380 kilobars was obtained for Young's modulus in the <100> direction, and a minimum of 1750 kilobars for the

<111> direction. They[63] stated that Young's modulus and shear modulus values of polycrystalline UO_2 with zero porosity should lie between the Reuss average (2170 and 814 kilobars) and the Voigt average (2440 and 933 kilobars).

D. Elastic Modulus and Internal Friction of Ceramic Materials

Willmore et al.[44] stated that the elastic modulus of fireclay refractories is a better indication of changes in firing treatment than modulus of rupture, porosity, or firing shrinkage. Coble and Kingery[64] found that the effect of porosity on the elastic modulus of Al_2O_3 at room temperature agreed with the theoretical relationship derived by Mackenzie.[65] Fenstermacher and Hummel[66] related the strength and elastic modulus of mullite bodies at room temperature by the expression

$$S = (6.987 \times 10^{-4})E + 6588. \tag{8}$$

Spriggs[67] and Spriggs and Brissette[68] suggested an exponential expression to relate elastic modulus to porosity and stated that Poisson's ratio for polycrystalline alumina bodies was expressed by

$$\mu = 0.257 - 0.35P, \tag{9}$$

where

μ = Poisson's ratio,

and

$$P = \text{Volume-fraction porosity} = \frac{\text{Void volume}}{\text{Total specimen volume}}.$$

The exponential expression mentioned above was improved by taking into consideration the individual effects of open and closed pores.[69] The relationship proposed was

$$E = E_0 e^{-b_0 P_0 - b_c P_c}, \tag{10}$$

where E is the elastic modulus of porous polycrystalline specimen, E_0 is the elastic modulus of nonporous polycrystalline specimen, P is the volume fraction of open pores, P_c is the volume fraction of closed pores, and b_0 and b_c are empirical constants.

Knudsen,[70] using results published by different investigators on the study of Young's modulus of polycrystalline alumina, arrived at the expression

$$E = 4102e^{-3.95P}. \tag{11}$$

Hasselman[71] observed that the equation proposed by Spriggs[67,69] failed to satisfy the boundary condition. To obviate this shortcoming, he proposed an expression obtained by solving the relation given by Hashin[72] for the case in which the second phase was porosity. Recently, Hasselman's Equation[71] was extended[73] to differentiate between the different types of porosity, namely, at the grain boundaries, contained within grains, and even the shape of the pores. The expression becomes

$$E = E_0\left[1 - \frac{\sum_{i=1}^{i=n} A_i P_i}{1 + (A_i - 1)\sum_{i=1}^{i=n} P_i}\right], \tag{12}$$

where E is the elastic modulus of porous polycrystalline specimen, E_0 is the elastic modulus of nonporous polycrystalline specimen, P is the volume-fraction porosity, A is a constant, i represents the type of porosity, and n is the number of types of porosity.

Theoretical equations[72,74] were compared with the experimental values of Young's modulus of elasticity of ZrC containing a disperse phase of graphite.[75] For this system, Hashin's expression[72] provided the best fit. Hasselman[76] suggested that when porosity is the only variable, Young's modulus may be related to strength in a linear manner. He introduced the concept of stress-free material, which can be considered as being located above and below the pores in the direction of the applied stress. This investigator suggested that the effect of porosity on strength and Young's modulus can be expressed by

$$S = S_0(1 - A_S P), \tag{13}$$

and

$$E = E_0(1 - A_m P), \tag{14}$$

where A_S and A_m are constants, P is the volume-fraction porosity, and the terms $(1 - A_S P)$ and $(1 - A_m P)$ can be interpreted as the fraction of material able to carry the applied load. The decrease in the elastic constants with increased porosity of ThO_2 was reported[77] to be greater than the values obtained from theoretical equations.[65,72,78,79] This was attributed to the fact that the pores were not spherical and to the effects of other variables such as grain size, grain orientation, and grain boundary condition. Atlas[80] reported that for Al_2O_3, a plot of the log of Young's modulus against porosity gave a straight line with a slope of approximately 3.3. Marlowe and Wilder,[42] studying yttrium oxide, obtained a linear relationship between elastic modulus and porosity. Hanna[81] observed that Young's modulus for polycrystalline magnesia alumina spinel increased as the porosity decreased.

The anelastic properties of metals have been studied extensively, and a good review has been written by Zener.[13] For oxide ceramic materials, the amount of work is considerably less. Hanna and Crandall[82,83] observed that the internal friction of MgO increased as the grain size became smaller. This behavior was corroborated for yttrium oxide.[42] The results published by Southgate[84] on the internal friction of single crystals of MgO, indicating a lower damping than for polycrystalline MgO, confirm the results mentioned above. Recently, the dependence of internal friction upon temperature, frequency, porosity, and textural damage on several ceramic materials, including electrical porcelain, fireclay, refractory bricks, and whiteware, was studied.[85]

Considerable work has been performed on the elasticity and anelasticity of ceramic materials at high temperature. However, since the present investigation is concerned with measurements at room temperature, only a general description of these works will be made. Marlowe and Wilder[86] have published a comprehensive review on this subject. The elastic modulus normally decreases as the temperature increases. In polycrystalline alumina, a sharp deviation in the linearity of elastic modulus-temperature curves at about 1100°C was observed.[87] The same test, performed on single crystals, did not show this behavior. The results of the anelastic studies[87] indicate that this departure from linearity was due to grain-boundary relaxation. The elastic modulus of GeO_2 increased with temperature from about -120 to 400°C, and for SiO_2 from about -190 to 1175°C.[88] Roberts[89] suggested that the increase with elastic modulus observed in some refractory materials can be attributed to the occupancy of voids by the phase with the highest coefficient of expansion. Minor additions of Cr_2O_3 and La_2O_3 produced additional peaks in the internal-friction spectrum of Al_2O_3.[36] Wachtman determined the motion mechanism of oxygen vacancies around an impurity atom by measuring the mechanical and electrical relaxation in 98.5 m/o ThO_2 plus 1.5 m/o CaO specimens.[90] Anelastic studies elucidated that the pairing of interstitial titanium ions was the type of defect in vacuum-reduced rutile.[91]

III. SCOPE OF INVESTIGATION

The variables studied in the present investigation were oxygen-to-uranium (O/U) ratio, grain size, and density. The investigation of the effect of an excess of oxygen on the elastic and anelastic traits of uranium oxides was deemed interesting in the light of the results published by several workers. The O/U ratio has been reported to have a large influence on the plasticity of uranium oxides.[60,92] Scott et al.[60] indicated that a change in the O/U ratio from 2.00 to 2.16 caused a decrease of 34% in the elastic modulus. Kingery,[93] Nichols,[94] and Ross[95] concurred in that the thermal conductivity of nonstoichiometric samples was much lower than that for the stoichiometric compositions. Schaner[96] stated that a small amount of excess oxygen resulted in a large increase in the hardness of nonstoichiometric uranium oxides.

Grain size was selected as another variable because several workers reported that there was a relationship between this parameter and internal friction.[42,82,83]

In general, to have a high uranium atom concentration, uranium oxide bodies should be as dense as possible. However, under production conditions small fluctuations in density cannot be precluded. This made the investigation of the change of the elastic and anelastic traits within a small density range in the upper density region a worthwhile and significant subject of study.

IV. EQUIPMENT

The Förster method[24] was employed throughout this investigation for determining the elastic and anelastic properties. A schematic diagram of the apparatus and a view of the equipment are presented in Figs. 1 and 2, respectively. The characteristics of the components are listed in Appendix A. The main factors in the selection of the oscillator, power amplifier, driver, and pickup were their good frequency response and low noise. The features desired in the vacuum-tube voltmeter were its accuracy and low noise. The storage oscilloscope had the advantage over a conventional oscilloscope and camera of simplicity in recording the decay and the saving in the cost of film.

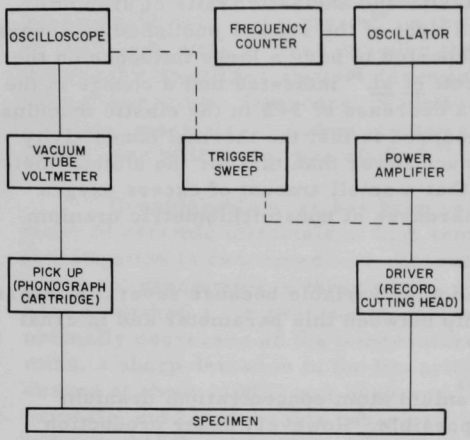

Fig. 1. Block Diagram of Apparatus for Elastic-modulus and Internal-friction Measurements

The transducers were mounted in the frame shown in Fig. 3, which was made of steel

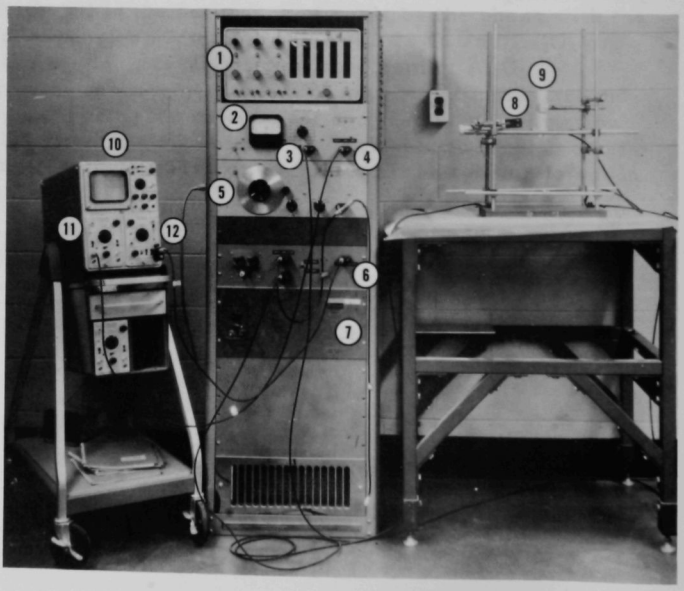

1. Frequency Counter
2. Vacuum-tube Voltmeter
3. Input Vacuum-tube Voltmeter
4. Output Vacuum-tube Voltmeter
5. Oscillator
6. Trigger Sweep
7. Power Amplifier
8. Driver
9. Pickup
10. Storage Oscilloscope
11. Amplifier (Plug-in unit)
12. Time Base (Plug-in unit)

Fig. 2
Equipment for Elastic and Anelastic Studies

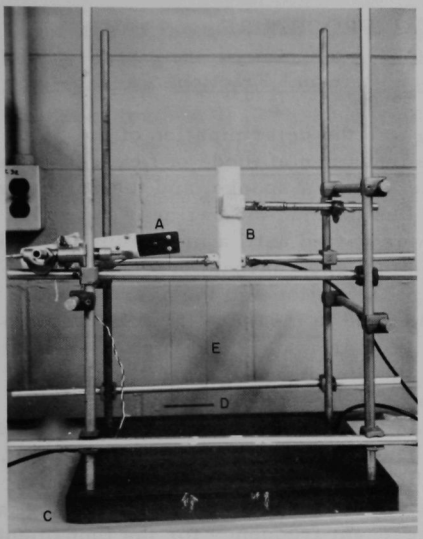

42532

A. Driver
B. Pickup
C. Brass Plate
D. Sample
E. Cotton Thread

Fig. 3. Transducers and Mounting Frame

rods screwed into a brass baseplate 3.5 cm thick. This system proved to be the most adequate for reducing vibrations transmitted from the floor. An Astatic cutting needle CL-92-3 was used in conjunction with the driver, and an Astatic needle N4-3S with the pickup. Cotton threads proved to be the best means of coupling the transducers to the specimen. This type of contact gave better results than touching the specimen directly with the needles, which tended to produce erratic internal-friction readings, depending on the pressure applied between the transducers and the sample.

The specimens were sintered in a hydrogen furnace. The samples were finished to the desired size with the help of a jig specially designed for this purpose. The device and the technique are explained in Appendix B.

V. EXPERIMENTAL PROCEDURE

A. Determination of Elastic Modulus and Internal Friction

The first step in the procedure was the determination of the approximate resonant frequency of the fundamental mode of flexural vibration. The uranium oxide specimen was laid on a sponge, and the driver and pickup were positioned so that the needles touched the bar near the ends. The frequency of the incoming signal was varied until a maximum deflection in the vacuum-tube voltmeter indicated that one resonant frequency of the specimen had been detected. The type of vibration and the overtone were determined next. The oscilloscope was used to measure this effect. Two identical amplifiers were plugged into the horizontal- and vertical-plate inputs of the scope. The signals from the pickup and the oscillator were fed into the vertical and horizontal plates, respectively, producing a Lissajou pattern. This figure shifted as the pickup was moved by hand from one end of the bar to the other, each change indicating a node of vibration. In the fundamental mode of flexural vibration there are two nodes; therefore the Lissajou pattern shifted twice when the specimen was vibrating in the appropriate frequency. Once the resonant frequency for the fundamental mode of flexural vibration was obtained for one bar it was not necessary to repeat the procedure for the rest of the specimens. Since the dimensions of all the samples were nearly the same, the resonant frequency was of the same order of magnitude throughout. The elastic modulus and internal friction were determined accurately by hanging the specimens from the needles of the driver and pickup by using cotton threads as coupling. The frequency of the oscillator was set in the range of the expected value and varied slowly back and forth. The resonant frequency was the one that produced a maximum deflection on the vacuum-tube voltmeter. The elastic modulus was calculated from this value, together with the dimensions and mass of the specimen. The rectangular cross section of the samples permitted two calculations of the elastic modulus (flatwise and edgewise), depending on which side was perpendicular to the direction of vibration. Failure to obtain a close agreement in both values was an indication of error in the calculations or a lack of isotropy and/or homogeneity in the bar. An example of the calculations is given in Appendix C.

The internal friction was detected by the logarithmic decay of vibrations when Q^{-1} was smaller than 10^{-3}, and by the half-bandwidth technique for high damping. The storage oscilloscope was employed for determining the decay of the amplitude of vibrations. An amplifier was plugged into the vertical-plate input, and a time base into the horizontal-plate input. The signal produced by the pickup was fed into the amplifier, and a trigger sweep (Fig. 1) was connected to the external trigger poles of the time base. The function of the trigger sweep was to cut off the excitation being fed into the driver while simultaneously starting a single sweep on the oscilloscope. The positions of the switches are indicated in Table III.

The decay of the amplitude of vibrations was displayed on the oscilloscope by depressing the switch of the trigger sweep, and was recorded by manual tracing.* An example of the calculation of the internal friction (Q_m^{-1}) using the decay method is given in Appendix D. Two determinations of Q_m^{-1} were made with the coupling at different distances from the end of the bar. These values and the expression given by Wachtman and Tefft[46] were used to determine the absolute internal friction of the sample (Q_s^{-1}). An example is given in Appendix D.

TABLE III. Position of Switches in Storage Oscilloscope for Determining the Decay of the Amplitude of Vibrations

Unit	Switch	Position
Cathode-ray tube	UPPER DISPLAY	STORE
	LOWER DISPLAY	STORE
Time base	MODE	Single sweep.
	LEVEL	Adjusted by hand to approximately zero.
	SLOPE	POSITIVE
	COUPLING	DC
	SOURCE	EXTERNAL

NOTE: After each determination, the MODE switch was reset.

The internal friction from the half-bandwidth of the resonant peak was also determined. An example of the calculation is given in Appendix D. The value of the background noise (A_B) was recorded. The resonant frequency (f_r) was determined, and the amplitude (A_R) of the signal at this point was read. The amplitude of the background (A_B) was subtracted from this value to give the true amplitude (A_T) at resonance. The frequency was reduced until the reading (A_{HB}) on the vacuum-tube voltmeter was equal to one-half the true amplitude plus the background amplitude (A_B), and this frequency was recorded. The frequency was increased again until the same reading (A_{HB}) was obtained on the vacuum-tube voltmeter, and the new frequency was noted. The difference between these frequencies at half the true amplitude gave the value of the half-bandwidth of the resonant peak. From this value and the resonant frequency the internal friction (Q_m^{-1}) was calculated.

*Kodak Topographic Sheet, Type A, was used for tracing.

B. Study of Effect of Density on Elastic Modulus and Internal Friction

The same lot of uranium dioxide* ceramic-grade powder was used for all the samples. The characteristics of the material are indicated in Table IV. The starting material was wet-mixed with 2% Carbowax,** granulated through a 20-mesh screen, pressed in a steel die at 140 kg/cm^2, and repressed isostatically at 3850 kg/cm^2. This technique minimized the stress gradient in the bars. The specimens were placed in a molybdenum boat, and the binder was burned out at 500°C in flowing hydrogen. The sintering was performed in hydrogen. The amount of carbon after sintering increased to 81 ppm, and the fluorine decreased to 66 ppm. Sintering temperature varied from 1750 to 1550°C, according to the density desired. The bars were brought to final dimensions by lapping. The technique is described in Appendix B. The faces were flat and parallel within 0.002 cm. Such precision is necessary to obtain correct absolute values of the elastic modulus. When relative changes of elastic modulus are determined by changing a variable within the same specimen, such accuracy in the dimensions is not necessary because the dimensional terms cancel out in the final equation. Approximate dimensions of the bars after sintering were 0.7 x 0.5 x 7 cm and, after finishing, 0.3 x 0.2 x 7 cm.

TABLE IV. Characteristics of UO_2†

Element	Parts/million	Element	Parts/million
A. Impurities			
Ag	<1	Li	<5
Al	20	Mg	15
As	<20	Mn	4
B	<0.1	Mo	<10
Be	<0.5	Na	30
Bi	<1	Ni	50
C	44	P	<50
Ca	<50	Pb	2
Co	<5	Sb	<2
Cr	40	Si	40
Cu	2	Sn	<5
F	260	Ti	<100
Fe	100	Zn	<50
K	<100		
B. Average particle size: <0.5 micron			
C. Surface area: 2.74 m^2/g			
D. O/U ratio: 2.05			

†Depleted Kerr-McGee Ceramic Grade.

*Kerr-McGee, Lot 1-30-36.
**Carbowax 4000.

The density was determined by the Archimedes method. The liquid used for the measurement was carbon tetrachloride. The elastic modulus and internal friction were calculated as described in Part A.

C. Study of Effect of Grain Size on Elastic Modulus and Internal Friction

The samples were pressed as explained in Part B, sintered in hydrogen at 1700°C for 2.5 hr, and finished as explained in Appendix B. A piece of one bar was cut and used to find the grain size. This value was assumed to be the same in the rest of the bars. This approximation seems reasonable because the samples were fabricated identically and sintered at the same time. The grain size was determined by the intercept method explained by Hilliard.[97a] Better results were obtained by making the measurements on the microscope image than on photomicrographs. Slightly changing the focus made it possible to distinguish some grain boundaries that were not otherwise readily discernible. After the elastic and anelastic traits were determined, the samples, together with the bar used for determining the grain size, were heat-treated in hydrogen to produce grain growth. After each heat treatment, the elastic modulus, internal friction, and grain size were again determined.

D. Study of Effect of Oxygen-to-Uranium Ratio

The stoichiometric bars were prepared as discussed in Part B. The O/U ratio after sintering was determined by oxidizing one of the samples to U_3O_8, measuring the weight gain, and assuming that the same O/U ratio was valid for the other samples. The bars were oxidized by placing the specimens and green pellets of U_3O_8 in sealed fused-silica tubes, which had been previously evacuated and then filled with argon at a partial pressure of 500 Torr. A piece of one bar, which had been prepared in a similar way as the specimen to be tested, was placed in each capsule. Figure 4 shows one of the capsules. The sealed tube was placed in a furnace, and the temperature was raised to 1100°C and held there for a period depending on the O/U ratio desired. The furnace was turned off and when the temperature was 450°C, the capsule was withdrawn and allowed to cool at room temperature. This cooling schedule produced a precipitation of a second phase. In a few cases, the specimens were taken out of the furnace at a different temperature to change the amount of the second phase precipitated. After the oxidation was completed, the O/U ratio was determined as a function of the known initial O/U ratio and the weight gain. Examples of the calculation of the O/U atom ratio are given in Appendix E. The specimens were tested to determine the elastic modulus and internal friction values. Some of the bars were oxidized further, and the steps were repeated.

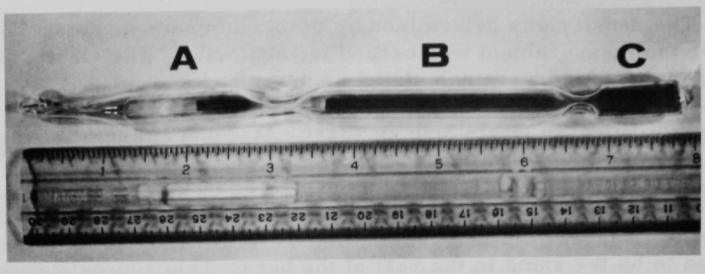

A. Piece for analysis
B. Sample for testing
C. U_3O_8 pellets

Fig. 4. Fused-silica Capsule for Oxidation of UO_2

E. Preparation of Polished Sections

The samples were mounted in cold-mount resin.* They were ground with 120, 240, 400, and 600 silicon carbide papers and polished with 6 μ and 1 μ diamond paste. A final polishing was given with 0.3 and 0.05 μ alumina. The specimens were etched with a solution of 10% H_2SO_4 and 90% H_2O_2.

F. X-ray Diffraction

The X-ray diffraction analysis was carried out by the Debye-Scherrer method. Powder patterns were taken by using CuKα radiation with a General Electric unit working at 15 mA and 48 kV peak. The diameter of the camera was 114.59 mm.

*Koldmount manufactured by Vernon-Benshoff Company.

VI. RESULTS AND DISCUSSION

A. Effects of Density on Elastic Modulus of Uranium Dioxide at Room Temperature

The change of elastic modulus with porosity of uranium dioxide at room temperature is shown in Table V and Fig. 5. All the specimens were stoichiometric. Figure 5 indicates the sensitivity of the technique employed. Although the density range covered was narrow, the elastic modulus clearly increased with density. The elastic modulus of nonporous uranium dioxide at room temperature was determined by the least-squares solution of Equation (14) and

$$E = E_0 e^{-bP}, \tag{15}$$

where E is the elastic modulus of the porous polycrystalline material, E_0 is the elastic modulus of the nonporous polycrystalline material, b is an empirical constant, and P is the volume-fraction porosity.

TABLE V. Elastic Modulus of Uranium Dioxide as a Function of Density

Sample	E_f, kilobars[a]	E_e, kilobars[b]	E_{av}, kilobars[c]	Density, g/cc	Percent of Theoretical Density[d]	Volume-Fraction Porosity
1	2056	2070	2063	10.53	96.07	0.0373
2	2062	2062	2062	10.61	96.80	0.0320
5	2067	2067	2067	10.73	97.90	0.0210
13	2048	2051	2099	10.63	96.99	0.0301
24	1920	1918	1919	10.53	96.07	0.0393
30	1888	1910	1899	10.41	94.98	0.0502
32	2069	2136	2102.5	10.52	95.98	0.0402
34	2127	2180	2155	10.72	97.81	0.0219
36	2105	2121	2113	10.66	97.26	0.0274
37	2151	2132	2142	10.73	97.90	0.0210
39	2108	2078	2094	10.63	96.99	0.0301
44	2090	2070	2080	10.57	96.44	0.0356
45	1972	2026	1999	10.54	96.16	0.0384
46	2149	2086	2188	10.59	96.62	0.0338
47	2099	2075	2087	10.62	96.90	0.0310
48	2070	2045	2058	10.56	96.35	0.0365
49	2090	2076	2083	10.55	96.26	0.0374
50	2032	2049	2041	10.58	96.53	0.0347
68	2054	2061	2057	10.55	96.26	0.0374
71	2086	2073	2080	10.62	96.90	0.0310
74	1998	1987	1992	10.35	94.43	0.0557
75	1927	1935	1931	10.32	94.16	0.0584
76	1940	1948	1949	10.32	94.16	0.0584
68-1	2101	2093	2097	10.67	97.35	0.0265
68-2	2112	2104	2108	10.70	97.63	0.0237
69-1	2034	2025	2029	10.61	96.75	0.0325
69-2	2041	2030	2035	10.63	96.99	0.0301

[a] E_f is the elastic modulus calculated from flatwise flexural vibrations.
[b] E_e is the elastic modulus calculated from edgewise flexural vibrations.
[c] E_{av} is the average elastic modulus.
[d] The theoretical density of UO_2 used for the calculations was 10.96 g/cc.

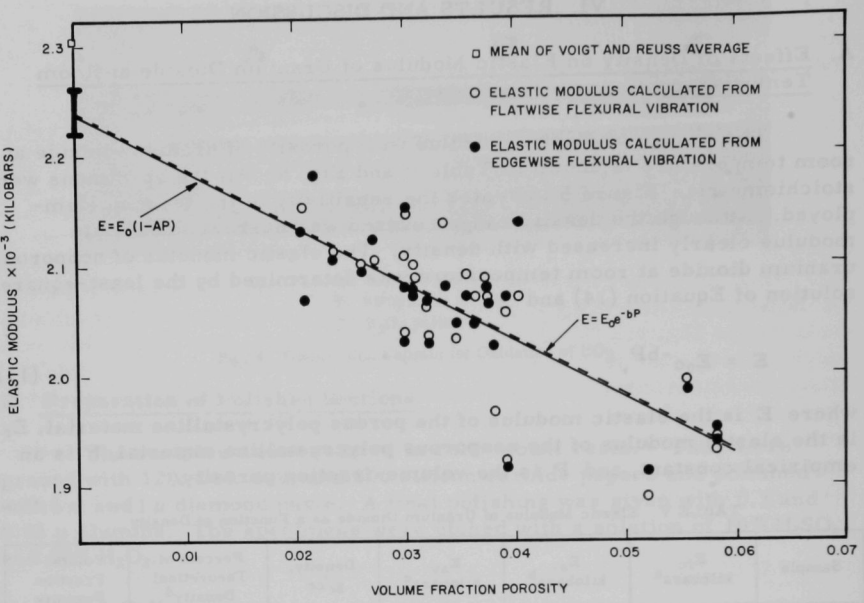

Fig. 5. Effect of Porosity on Elastic Modulus of UO_2 at Room Temperature

Equation (15) has been proposed by Spriggs[67] and is based on a relation between strength and porosity postulated by Knudsen.[98] Equation (15) may also be written

$$\ell n\, E = \ell n\, E_0 - bP, \tag{16}$$

which is easier to solve by the least-squares method. The values for E_0, b, and A are presented in Table VI. The values obtained for E_0 fall within the range mentioned by Wachtman et al.,[63] who determined that Young's modulus for nonporous polycrystalline UO_2 without preferred orientation should be between 2170 kilobars (Reuss average) and 2440 kilobars (Voigt average). The mean of both averages is 2305 kilobars. The agreement with the present data is good, even better if one realizes that (a) the techniques employed were dissimilar, (b) Equations (14) and (15) are based on ideal conditions that are not always attained in practice, and (c) some error is introduced during the density determination. Wachtman et al.[63] worked in the ultrasonic region; in the present investigation, the tests were performed by Förster's method in the sonic range. The same authors[63] claim that, by extrapolating the results published by Lang,[62] a value of 2280 kilobars is obtained for nonporous uranium dioxide. This agrees even more closely with the present results. Some of the specimens used by Lang[62] were not stoichiometric.

TABLE VI. Values of E_0, b, and A Obtained by Least-squares Fitting of Exponential and Linear Equations

Equation	E_0, kilobars	b	A
$E = E_0 e^{-bP}$	2243.56 ± 22.10	2.512	-
$E = E_0(1 - AP)$	2233.85 ± 22.05	-	2.277

By the use of the least-squares fitting of data, the elastic modulus was calculated from zero to 0.4 volume-fraction porosity. The results are presented in Fig. 6. The information in the literature has also been plotted. These values, in general, follow closely the curve obtained by fitting the linear equation proposed by Hasselman.[76] The lower value obtained by Lambertson and Handwerk[56] should be attributed to the static technique employed, which produces smaller values for the elastic modulus (relaxed modulus). The very small deflections produced in uranium oxide, when subjected to a static load at room temperature, make it difficult to obtain precise results with this technique.

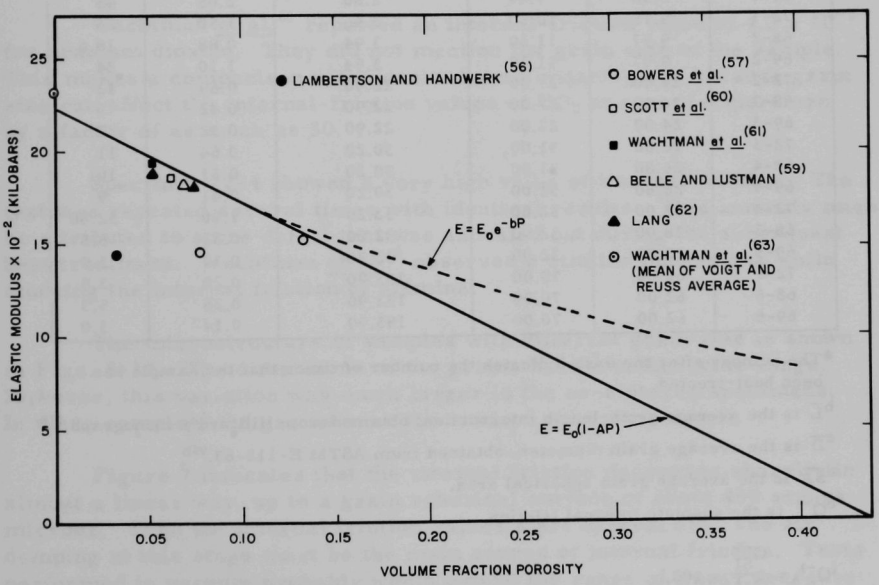

Fig. 6. Variation of Elastic Modulus of UO_2 at Room Temperature, Calculated from Exponential and Linear Relationships with Porosity

The exponential equation gives higher values of the elastic modulus. That is because, as mentioned before, this relation does not fulfill the boundary condition for P = 1. The linear equation gives zero elasticity for a volume-fraction porosity of 0.438. This is consistent with the postulate of Marlowe and Wilder[42] that a material of initial uniform particle size should approach zero elasticity at porosity less than 0.4764 volume-fraction porosity.

B. Effects of Grain Size on Internal Friction of UO_2

The variation of internal friction as a function of grain size of urania is presented in Table VII and Fig. 7.

TABLE VII. Internal Friction Against Grain-size Dimensions

Sample[a]	$\overline{L}$, microns[b]	$\overline{D}$, microns[c]	$\overline{SA} \times 10^{-2}$, square microns[d]	$Q_s^{-1} \times 10^4$[e]	Q_R^{-1}[f]
72	7.05	7.94	1.98	5.78	100
68	7.05	7.94	1.98	4.72	100
69	7.05	7.94	1.98	4.56	100
68-1	8.38	9.44	2.80	2.55	54
69-1	8.38	9.44	2.80	2.05	45
72-1	9.15	10.50	3.46	1.50	26
68-2	9.97	11.20	3.94	0.88	18.6
69-2	9.97	11.20	3.94	1.10	24
72-2	24.00	27.00	22.90	0.69	12
68-3	24.00	27.00	22.90	0.42	9
69-3	24.00	27.00	22.90	0.32	7
72-3	26.80	31.00	30.20	0.64	11
68-4	26.80	31.00	30.20	0.51	10
69-4	26.80	31.00	30.20	0.41	9
72-4	28.00	32.00	32.20	1.90	32.80
68-5	28.00	32.00	32.20	0.31	6.5
69-5	28.00	32.00	32.20	0.14	3.0
72-5	62.00	70.00	153.90	0.20	3.5
68-6	62.00	70.00	153.90	0.25	5.3
69-6	62.00	70.00	153.90	0.14	3.0

[a]The number after the dash indicates the number of times that the sample has been heat-treated.

[b]$\overline{L}$ is the average grain-length intersection, obtained from Hilliard's monograph.[97a]

[c]$\overline{D}$ is the average grain diameter, obtained from ASTM E-112-63.[97b]

[d]$\overline{SA}$ is the average grain spherical area.

[e]Q_s^{-1} is the absolute internal friction.

[f]$$Q_{RA}^{-1} = \frac{Q_{SI}^{-1}}{Q_{SA}^{-1}} \times 100,$$

where Q_{RA}^{-1} is the relative internal friction for a sample of grain size A; Q_{SI}^{-1} is the absolute internal friction for the initial sample, in this case with a grain diameter of 7.94 microns; and Q_{SA}^{-1} is the absolute internal friction for a sample of grain size A.

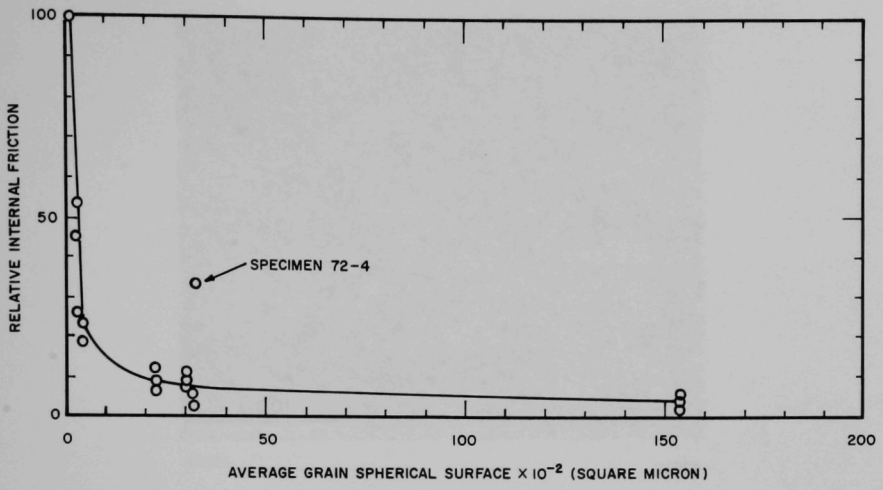

Fig. 7. Change of Internal Friction with Grain Dimensions

Wachtman et al.[61] reported an internal-friction value of 4.3×10^{-5} for uranium dioxide. They did not mention the grain size of the sample. This makes a comparison with results herein meaningless because grain size can affect the internal-friction values of UO_2 at room temperature by a factor of as much as 30.

Specimen 72-4 showed a very high value of internal friction. The test was repeated several times with identical results. This anomaly might be attributed to some defect that was annealed out during the subsequent heat treatment. Wachtman et al.[61] observed a similar phenomena while studying the internal friction of alumina.

The microstructure of samples with different grain size is shown in Figs. 8-11. The dimensions of the grains have a rather wide range. However, this variation was much larger in the as-sintered specimens. In these samples, the grains near the surface were very small.

Figure 7 indicates that the internal friction decreases sharply, in almost a linear way, up to a grain spherical surface of about 400 square microns. Then the internal friction values start to level off. The air damping at this stage must be the main source of internal friction. Tests performed in vacuum probably would extend the range of linear decrease of internal friction with increasing grain size.

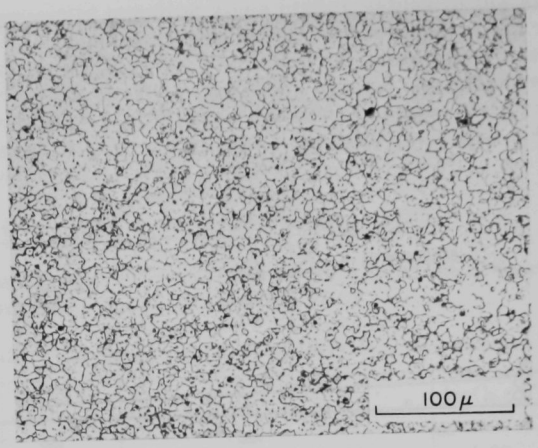

42612

Fig. 8. Microstructure of $UO_{2.005}$ with Average Grain Diameter of 7.94 μ, after Etching

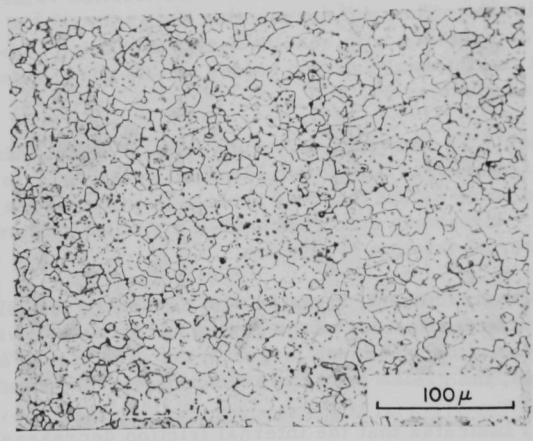

42613

Fig. 9. Microstructure of $UO_{2.005}$ with Average Grain Diameter of 11.2 μ, after Etching

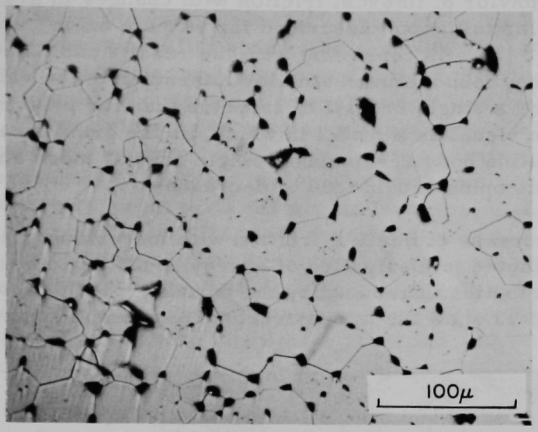

42614

Fig. 10. Microstructure of $UO_{2.005}$ with Average Grain Diameter of 32.4 μ, after Etching

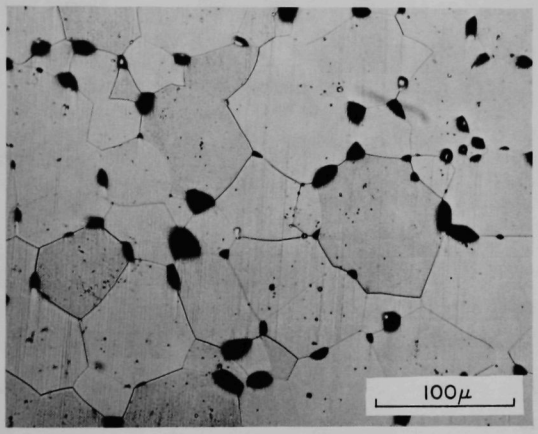

42615

Fig. 11. Microstructure of $UO_{2.005}$ with Average Grain Diameter of 70 μ, after Etching

The behavior of internal friction with changes in grain size follows a pattern similar to the one described for yttrium oxide[42] and for magnesium oxide.[82,83] This is consistent with the results published by Wachtman and Lam.[87] They found a much smaller internal-friction value at room temperature for a single crystal of sapphire than for polycrystalline alumina. One can visualize a model in which, as the grain size increases, the polycrystalline body resembles a single crystal more and more. Consequently the damping should tend to decrease.

The decrease of internal friction with increasing grain size is generally attributed to dissipation of energy at the grain boundaries. However, the contribution introduced by the porosity should also be considered. Figures 12 and 13 show the microstructure of two specimens with different

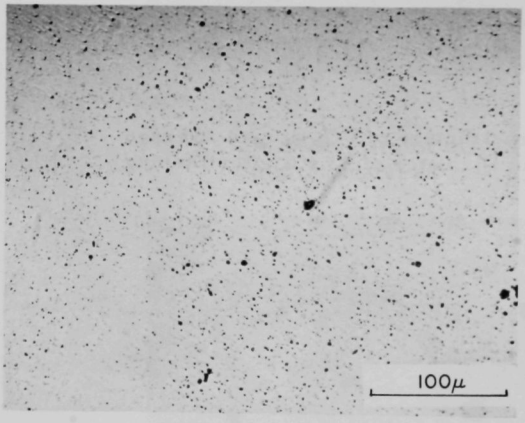

42616

Figure 12
Microstructure of $UO_{2.005}$ with Average Grain Diameter of 7.94 μ, before Etching

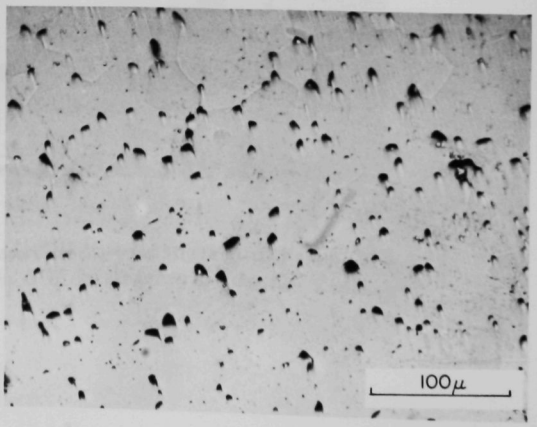

42617

Figure 13
Microstructure of $UO_{2.005}$ with Average Grain Diameter of 32.4 μ, before Etching

grain dimensions, before etching. When the grains are small, the porosity is scattered; but when the grains become larger, the number of pores is smaller, and then the possibility of interference with the elastic waves diminishes. A test was performed to produce some evidence that the whole microstructure should be considered in evaluating the internal friction. A specimen (No. 13) was sintered in such a way that the binder was not properly burned out. This produced a microstructure with many elongated pores at the grain boundaries (Fig. 14). The absolute internal friction of this sample was five times as large as for a specimen of similar grain size but without this type or porosity. This test seems to indicate that the number, size, and position of the pores has considerable influence on the internal friction at room temperature. Sample 13 had a free-carbon content about 2.7 times as large as that detected in a sample where the binder was properly burned out. This also might have some influence on the increase of the damping trait.

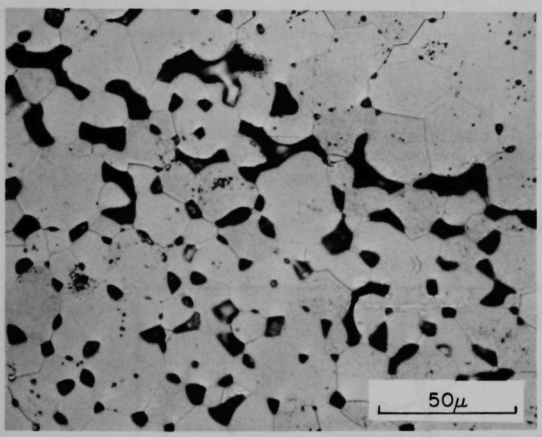

42618

Figure 14

Microstructure of $UO_{2.005}$ after Etching, Showing Elongated Porosity at Grain Boundaries

C. Effect of Oxygen-to-Uranium Atom Ratio on Elastic Modulus and Internal Friction of Uranium Oxides at Room Temperature

1. Effect of Oxygen Content on Elastic Modulus of Urania at Room Temperature

The first step was to determine the variation of elastic traits due to the oxidation of stoichiometric samples. The oxygen was introduced as explained in Section V-D. All the bars were withdrawn from the furnace at 450°C. The results of the change of elastic modulus with oxygen content of urania are shown in Table VIII and Fig. 15. As the oxygen content increased, the signal from the pickup became weaker, making the elastic results less accurate. This might account for the larger scattering encountered in the data for compositions with an O/U ratio greater

TABLE VIII. Effect of Oxygen on Elastic Modulus of Urania at Room Temperature

Sample[a]	O/U	E_{FR}[b]	E_{ER}[c]	Sample[a]	O/U	E_{FR}[b]	E_{ER}[c]
3	2.005	100	-	3-1	2.033	87.5	-
30	2.005	100	100	32-2	2.054	68.5	69
32	2.005	100	100	34-1	2.055	59.2	59.7
34	2.005	100	100	30-2	2.057	72	74.3
36	2.005	100	100	32-3	2.063	59	60
37	2.005	100	100	30-3	2.067	66.5	68.5
48	2.005	100	100	32-4	2.081	56	56
49	2.005	100	100	36-1	2.081	63.1	63.6
50	2.005	100	100	30-4	2.086	70	-
32-1	2.025	91.8	92.3	37-1	2.107	63.4	63.4
30-1	2.030	91.5	93	37-2	2.124	63.2	63.3

[a]The number after the dash indicates the number of times the sample was oxidized.

[b]$E_{FRA} = \frac{E_{FA}}{E_{FI}} \times 100$,

where E_{FRA} is the relative flexural elastic modulus of a sample having an O/U ratio of A; E_{FA} is the absolute flexural elastic modulus of a sample having an oxygen-to-uranium ratio of A; E_{FI} is the absolute flexural elastic modulus of a sample having the initial O/U ratio (2.005).

[c]Same as b, but for edgewise flexural elastic modulus.

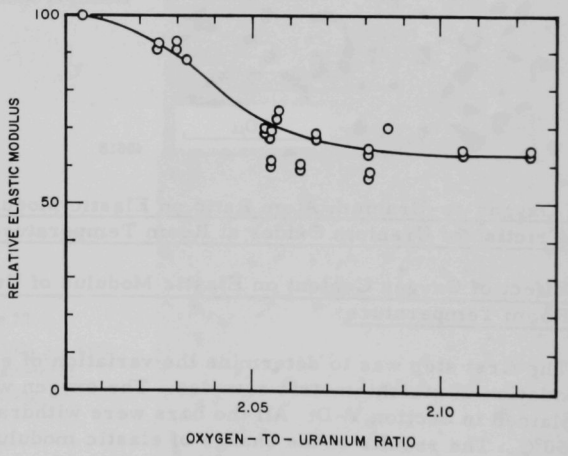

Fig. 15. Change of Elastic Modulus with Oxygen Content

than 2.05. Microstructures of specimens with different oxygen content are shown in Figs. 16-23. After the specimens were etched with a solution of 10% H_2SO_4 and 90% H_2O_2, a second phase was detected, which increased as the excess of oxygen became larger. Stoichiometric specimens (Fig. 19) did not show this second phase when etched. This ruled out that this microstructural aspect would have been produced by the H_2O_2 present in the etching solution. Attempts to identify the second phase as U_4O_9 were inconclusive. X-ray diffraction films of nonstoichiometric specimens contained extra lines compared with the films of stoichiometric samples. The presence of U_4O_9 is usually indicated by the appearance of strong lines with "d" spacings[99] of 0.7843 (α_1) and 0.7823 (α_2), joint contribution of UO_2 and U_4O_9; weak lines with "d" spacings of 0.7818 (α_1) and 0.7795 (α_2); and very weak lines with "d" spacings of 0.774 (α_1) and 0.773 (α_2). The X-ray

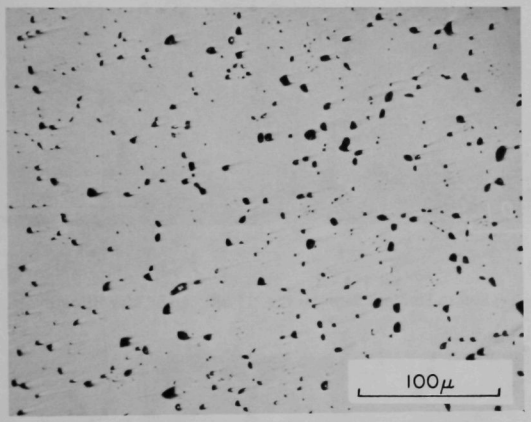

42619

Figure 16

Microstructure of $UO_{2.005}$, before Etching

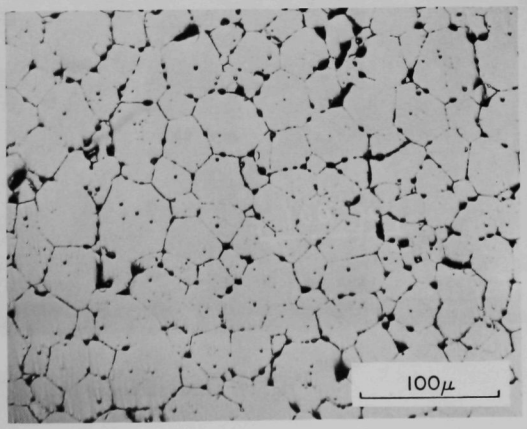

42620

Figure 17

Microstructure of $UO_{2.055}$, before Etching

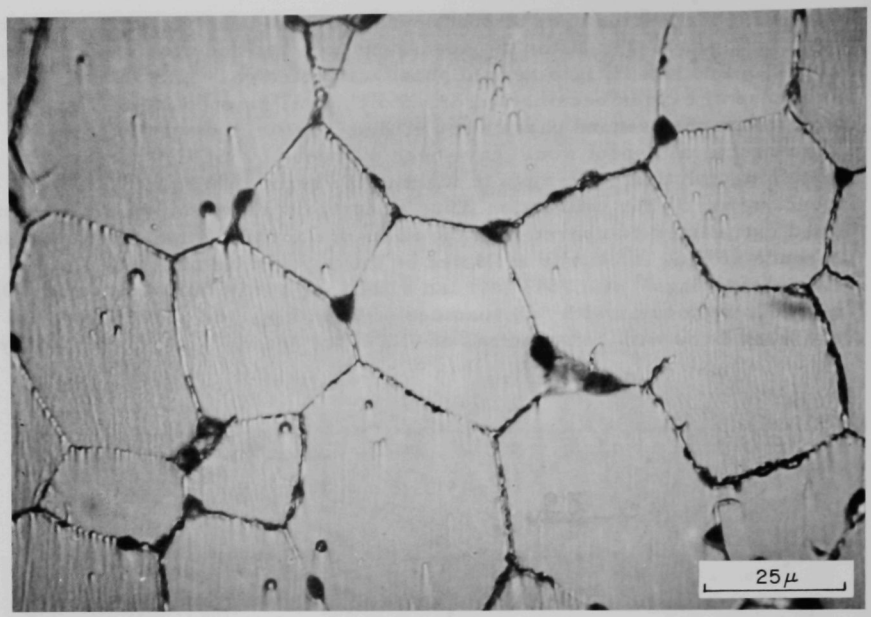

42621

Fig. 18. Microstructure of $UO_{2.055}$, before Etching; Same as Fig. 17 but Larger Magnification

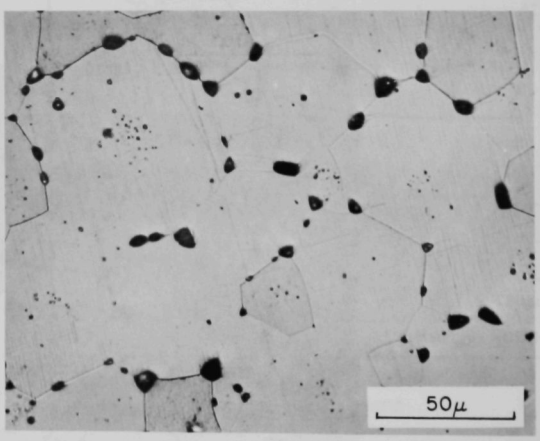

42768

Fig. 19. Microstructure of $UO_{2.005}$, after Etching

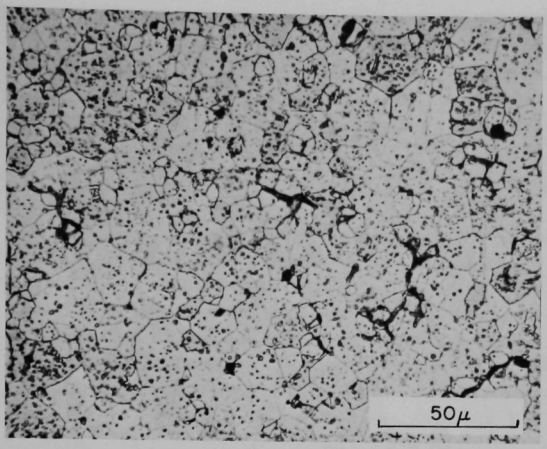

42769

Fig. 20. Microstructure of $UO_{2.033}$, after Etching

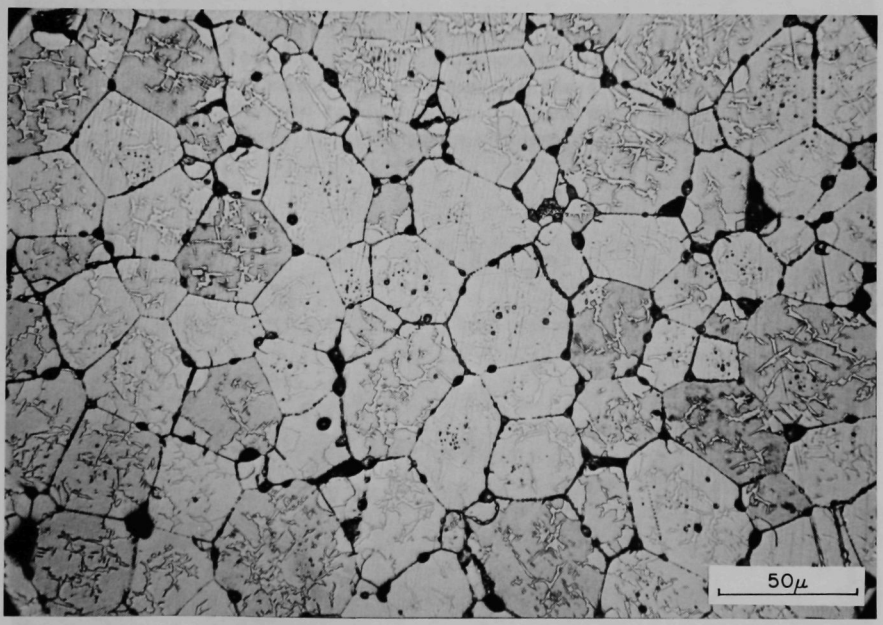

42770

Fig. 21. Microstructure of $UO_{2.055}$, after Etching

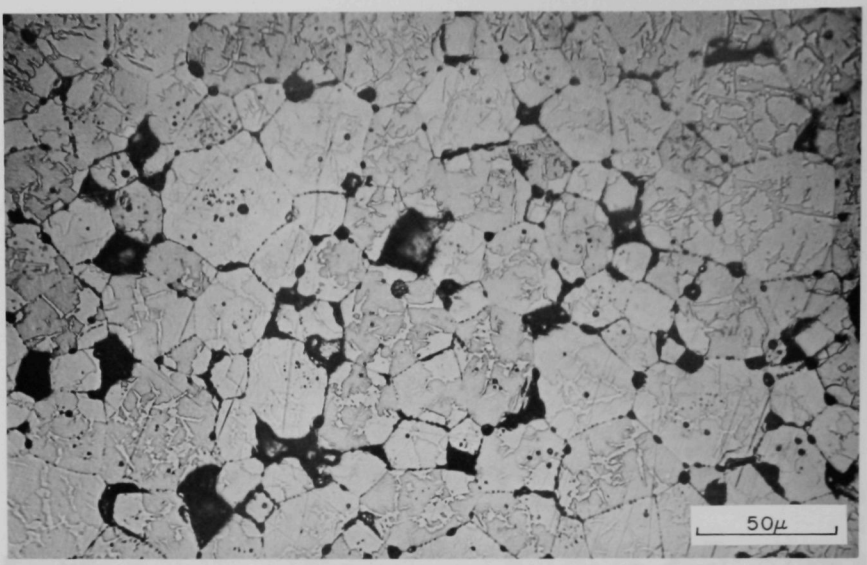

42771

Fig. 22. Microstructure of $UO_{2.081}$, after Etching

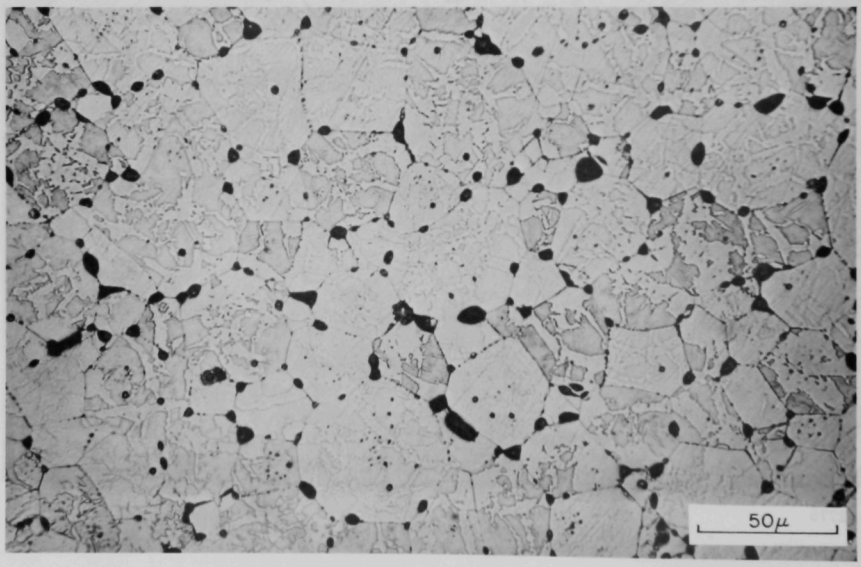

42772

Fig. 23. Microstructure of $UO_{2.107}$, after Etching

film of nonstoichiometric samples of composition $UO_{2.073}$ or larger contained weak lines corresponding to "d" spacings of 0.7859 (α_1) and 0.7841 (α_2). These and other extra lines at higher "d" spacings indicate the presence of two phases but do not permit their positive identification. However, the phase diagrams (Fig. 24) published by several workers[96,100-102] strongly indicate that the second phase must have been U_4O_9, probably with oxygen deficiency (U_4O_{9-y}), which had precipitated along the [111] plane during cooling, after introduction of oxygen.[96,102,103,104]

When the samples were hyperstoichiometric, the grain boundaries were visible before etching; for stoichiometric oxides, the grain contours were only visible after etching, as can be seen in Figs. 16-19. Probably during oxidation the oxygen diffused through the boundaries and pores. When UO_{2+x} was transformed into U_4O_9, the volume changed, and as a result a gap took place between the grains. The microstructure of the nonstoichiometric oxide (Figs. 20-23) shows that the U_4O_9 is spread around pores and triple-boundary joints. This seems to be consistent with the above premise. It is also interesting to observe the pores at the grain boundaries of the urania specimens having an excess of oxygen.

Figure 15 indicates that the elastic traits of urania decreased in a large degree up to a composition of $UO_{2.05}$ and then started to level off. Scott et al.[60] reported that the elastic modulus of a sample with composition $UO_{2.16}$ was 66.6% of the value of the same specimen with composition $UO_{2.00}$. That would agree with the present data, if the plateau observed in Fig. 15 remained unchanged to urania composition of $UO_{2.16}$, which seems a reasonable assumption.

The results may have been affected by an oxidation gradient in the samples. To clarify this point, bars were annealed at 1100°C, and the elastic modulus was determined again. The results shown in Table IX indicate that the elastic values did not change much with annealing. Comparison of Figs. 23 and 25 indicates that the microstructure was not affected by the annealing treatment. This might be due to two reasons: (a) during the cooling following annealing, the equilibrium previously attained was broken again, and (b) the samples had reached equilibrium by the completion of the oxidation treatment. To probe into the first possibility, one sample of composition $UO_{2.084}$ was left to cool very slowly in the furnace. The elastic modulus determination gave relative values of E_{FR} = 51.5 and E_{ER} = 52.4. These

TABLE IX. Relative Elastic Modulus before and after Annealing

Sample	O/U	Before Annealing		After Annealing	
		E_{FR}[a]	E_{ER}[b]	E_{FR}[a]	E_{ER}[b]
30-R	2.026	83	-	81	-
34-1	2.055	59.2	59.7	58	64
32-4	2.081	56	56	56.8	57
30-4	2.086	70	-	70	-
37-1	2.107	63.4	63.4	63.8	64

[a] $E_{FRA} = \frac{E_{FA}}{E_{FI}} \times 100$,

where E_{FRA} is the relative flexural elastic modulus of a sample with an O/U ratio of A; E_{FA} is the absolute flexural elastic modulus of a sample with an O/U ratio of A; E_{FI} is the absolute flexural elastic modulus of a sample with the initial O/U ratio (2.005).

[b] Same as a, but for edgewise flexural elastic modulus.

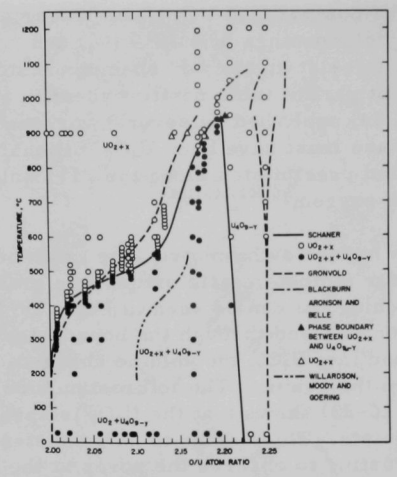

Figure 24

UO_2-U_4O_9 Phase Diagram (after Schaner[96])

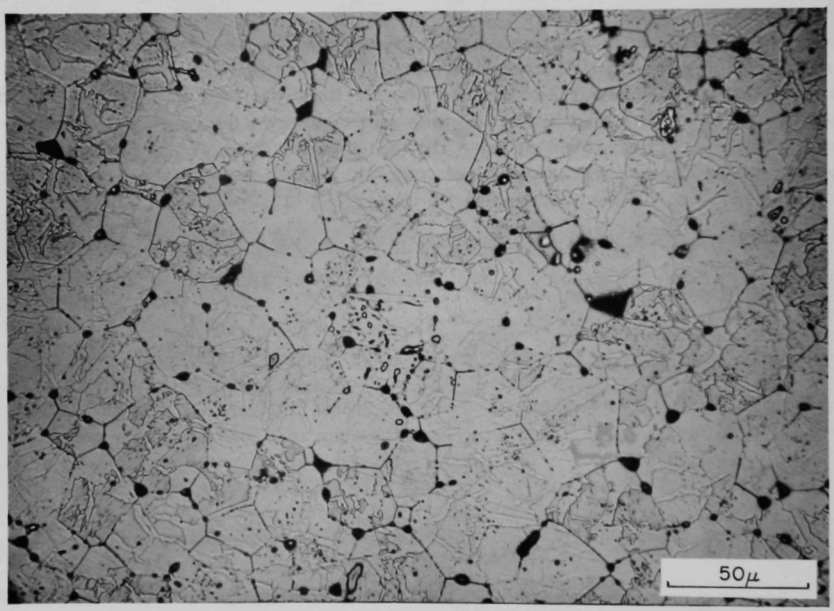

Fig. 25. Microstructure of $UO_{2.107}$, after Annealing and Etching

were somewhat less than the ones shown in Fig. 16. However, the difference was not very large, especially because at this stage of oxidation the weak pickup signal made the elastic determination less accurate. The second possibility arises because the oxygen used for the oxidation was supplied by the U_3O_8 powder and the rate of evolution must have decreased exponentially with time. The oxidation treatment of all the samples took more than 70 hr, and by this time the entire system must have reached a point of quasiequilibrium.

Figure 26 showed that intergranular cracks were present after oxidation. This immediately raised the question of whether the decrease of the elastic traits was the aftereffect of these microstructural defects or due to the excess of oxygen in the lattice. Two samples were reduced, and the elastic modulus was determined again. The results are presented in Table X. The microstructures of these specimens are shown in Figs. 26-28.

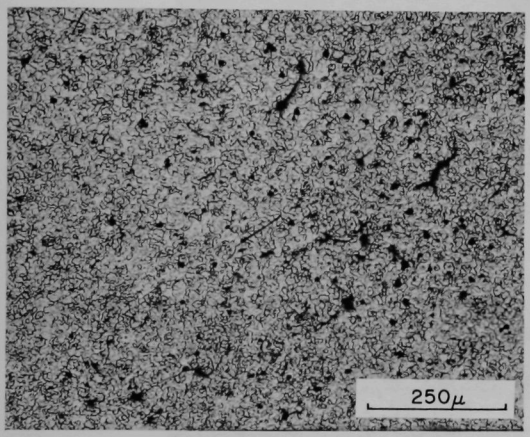

42631

Figure 26

Microstructure of $UO_{2.089}$, after Etching

TABLE X. Relative Elastic Modulus of Uranium Oxides Which Have Been Oxidized and Reduced

Sample	O/U	E_{FR} [a]	E_{ER} [b]	Remarks
32	2.005	100	100	Test was performed before any oxidation or reduction was made.
32-R	2.005	97	97	Oxidized to $UO_{2.081}$ and then reduced to $UO_{2.005}$.
30-R	2.026	83	-	Sample was oxidized to $UO_{2.086}$ and then reduced to $UO_{2.026}$.

[a] $E_{FRA} = \frac{E_{FA}}{E_{FI}} \times 100$,

where E_{FRA} is the relative flexural elastic modulus of a sample with an O/U ratio of A; E_{FA} is the absolute flexural elastic modulus of a sample with an O/U ratio of A; E_{FI} is the absolute flexural elastic modulus of a sample with the initial O/U ratio (2.005).

[b] Same as a, but for edgewise flexural elastic modulus.

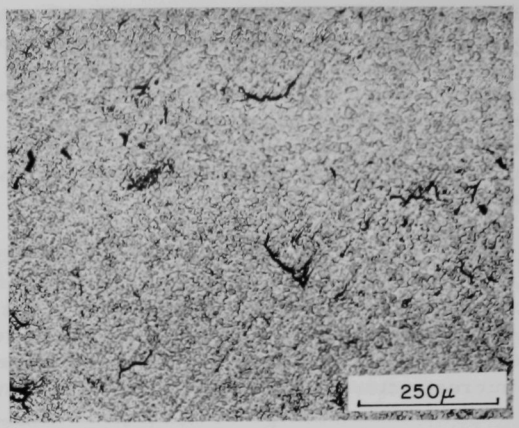

42630

Fig. 27. Microstructure of a Specimen Reduced from $UO_{2.089}$ to $UO_{2.005}$ (Same Specimen as in Fig. 26)

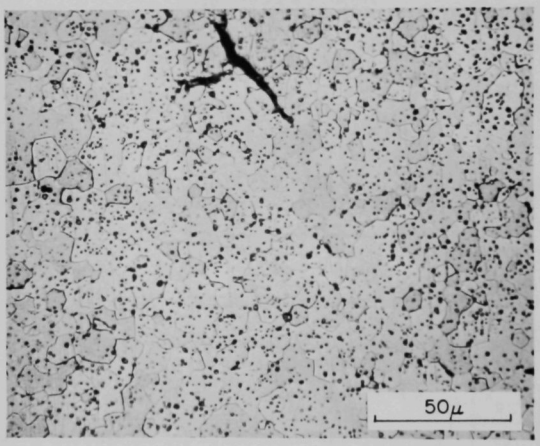

42773

Fig. 28. Microstructure of a Specimen Reduced from $UO_{2.089}$ to $UO_{2.005}$; Same as Fig. 27, but Larger Magnification to Show Absence of U_4O_9 Phase.

Table X showed that practically the same elastic values were obtained for the initial specimen and after oxidizing and reducing (samples 32 and 32-R). Figures 27 and 28 indicated that the cracks remained but the second phase was obliterated after reduction. The results of the elastic determination and metallographic work indicated that the decrease in the elastic modulus of UO_2 as the oxidation proceeded was due mainly to the presence of oxygen. Comparison of the Young's modulus of 30-R with the results presented in Fig. 15 corroborated this statement. The microstructure is shown in Fig. 29.

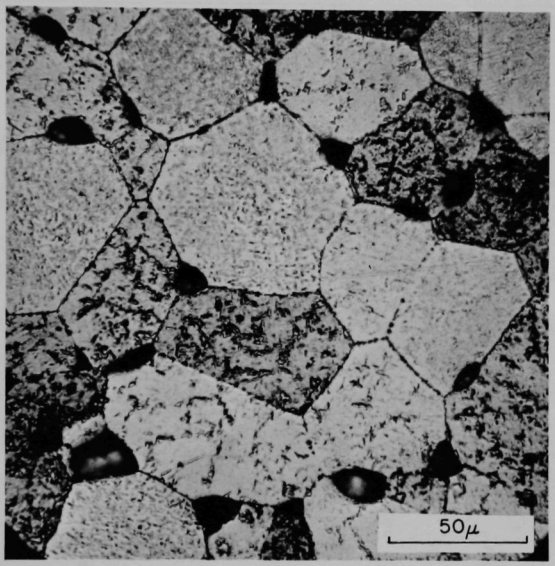

Fig. 29. Microstructure of a Specimen Reduced from $UO_{2.089}$ to $UO_{2.026}$, after Etching

The next point to make clear was whether the decrease in the elastic traits of urania with excess oxygen was due to the oxygen being in solid solution or to the U_4O_9 phase. Ross[95] expressed the same doubt while studying the thermal conductivity of uranium oxide. He attributed the thermal-conductivity behavior to the presence of a precipitated U_4O_9 phase in the nonstoichiometric samples, but he did not present proof of this. To answer the question, three bars (49-1, 50-1, and 48-1) were oxidized at 1100°C. Samples 49-1 and 50-1 were withdrawn from the furnace at 800 and 450°C, respectively; 48-1 was allowed to cool very slowly. The elastic modulus was determined, and the results are presented in Table XI. The microstructures of 49-1 and 50-1 are shown in Figs. 30 and 31. The elastic trait of 49-1 was much higher than for the

TABLE XI. Effect of Oxidation Schedule on Elastic Modulus of Uranium Oxide

Sample	O/U	E_{FR}[a]	E_{ER}[b]
49-1	2.071	86.3	-
50-1	2.073	53.4	54.3
48-1	2.084	51.5	52.4

[a] $E_{FRA} = \frac{E_{FA}}{E_{FI}} \times 100$,

where E_{FRA} is the relative flexural elastic modulus of a sample with an O/U ratio of A; E_{FA} is the absolute flexural elastic modulus of a sample with an O/U ratio of A; E_{FI} is the absolute flexural elastic modulus of a sample with the initial O/U ratio (2.005).

[b] Same as a, but for edgewise flexural elastic modulus.

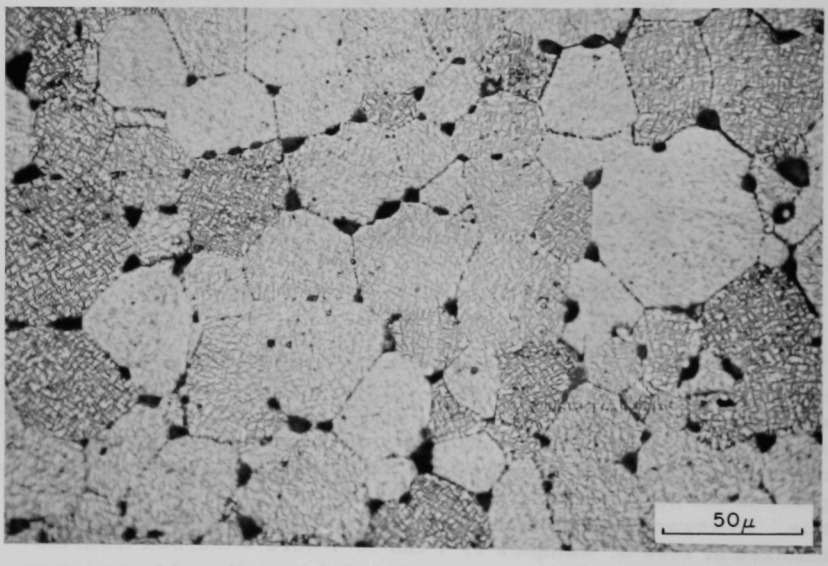

42627

Fig. 30. Microstructure of $UO_{2.071}$, after Etching, Oxidized at 1100°C and Quenched in Air at 800°C.

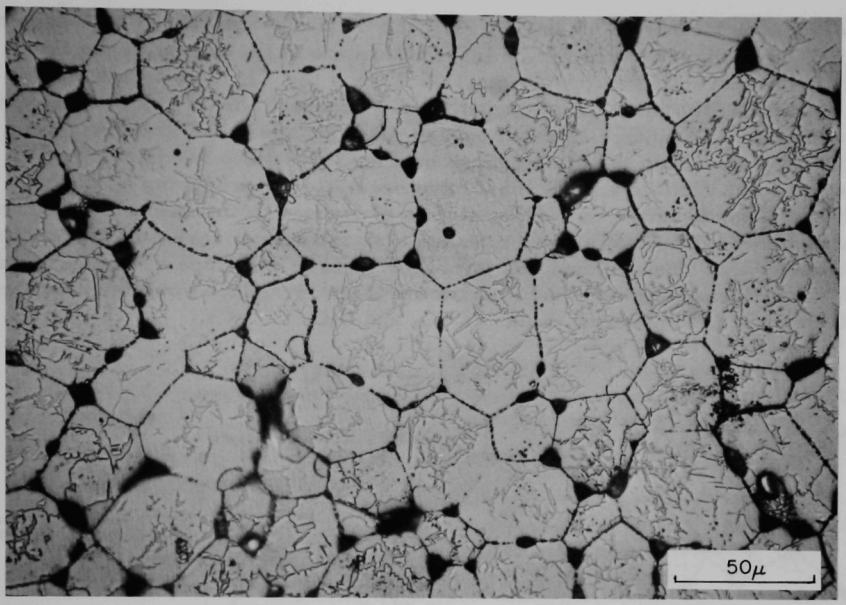

42628

Fig. 31. Microstructure of $UO_{2.073}$, after Etching, Oxidized at 1100°C and Quenched in Air at 450°C

other two samples. The microstructure of 49-1 presented a Widmanstätten structure; for 50-1, the second phase formed interconnected bands. The microstructure of 48-1 was similar to that of 50-1. This indicates[96,103] that the amount of U_4O_9 was greater in 50-1 and 48-1 than in 49-1, which was also qualitatively substantiated by the X-ray data. The pattern of 49-1 did not show lines with "d" spacings at 0.7859 (α_1) and 0.7841 (α_2), but for 50-1 and 48-1 these lines were present. The combination of the elastic modulus values and X-ray and metallographic studies established that the main cause for the observed behavior of the elastic traits of urania with oxidation was the presence of the U_4O_9 phase. The plateau observed in plotting the elastic modulus against oxygen content must be also attributed to the presence of U_4O_9. When the O/U ratio was greater than 2.05, the amount of U_4O_9 precipitated was such, due to the oxidation schedule chosen, that the elastic properties of the bar were similar to the ones of a body with 100% U_4O_9. Unfortunately, the exactitude of this assumption could not be verified because data were not found on the elastic modulus of U_4O_9.

Three possible types of oxygen atoms are present in the U_4O_9 structure.[105,106] The O atoms are the ones existing in the fluorite structure

of the stoichiometric oxide (Fig. 32), the O' atoms are placed 0.85 Å along the <110> directions from the large interstice at the center of the fluorite structure, and the O" atoms 1.05 Å along the <111> directions. The positions of the interstitial oxygen atoms are shown in Fig. 33. According to Willis,[106] the introduction of oxygen must change some uranium atoms from U^{+4} to U^{+5} to maintain charge balance (Fig. 34). The bonding strength and lattice energy must have been altered producing a change in the Condon-Morse curves (variation of force with interatomic distance), and consequently, the elastic modulus also must have varied because it is known[107] that Young's modulus is proportional to the slope of this curve at the equilibrium distance between atoms (Fig. 35). That would explain the difference in the elastic values of UO_2 and U_4O_9.

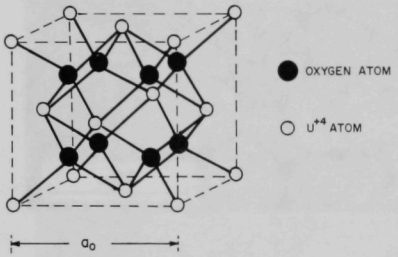

Fig. 32. Structure of Stoichiometric Uranium Oxide (Fluorite Structure)

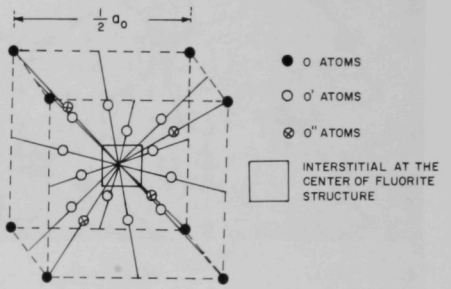

Fig. 33. Position of Oxygen Atoms in Cell of U_4O_9 (after Willis[106])

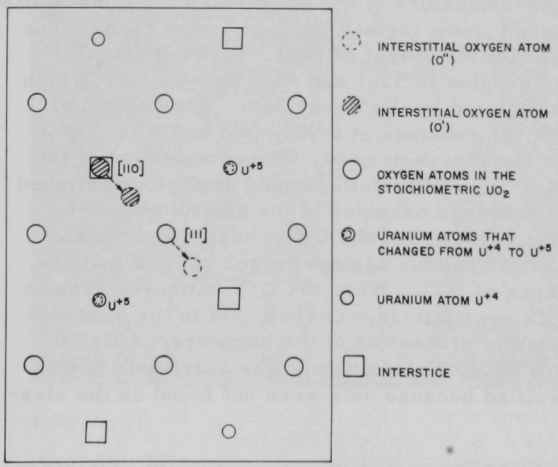

The interstitial atom O' enters the structure at the interstice and moves along the <110> direction because of the electrostatic attraction induced by two uranium atoms. These two atoms change valence to maintain charge balance. The repulsion force from O' displaces an O atom in an interstitial position along the <111> direction (O" interstitial oxygen atom).

Fig. 34. Diagram Indicating Changes in Uranium Oxide Lattice Produced by Introduction of Oxygen (after Willis[106])

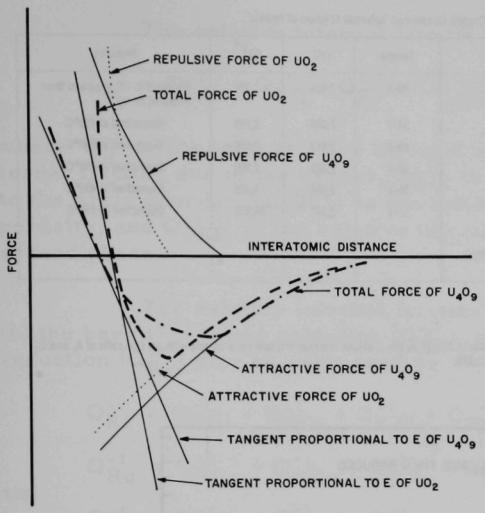

Fig. 35. Model of Condon-Morse Curves Indicating Reason for Difference between Elastic Moduli of UO_2 and U_4O_9

Assume that the elastic modulus of U_4O_9 is 50% of Young's modulus of UO_2. If the variation of elastic modulus with the ratio of UO_2 to U_4O_9 follows the pattern observed by Hasselman[75] for a two-phase material, a curve as shown in Fig. 36 would be obtained, which resembles the graph presented in Fig. 15. The plotting of the elastic traits at room temperature against the ratio of the two phases should produce an invariable curve; plotting the elastic modulus at room temperature against the O/U ratio would result in a curve depending on several variables, such as temperature of oxidation, quenching, and O/U atom ratio.

2. Effect of Oxygen Content of Urania on Internal Friction

The relative internal friction of uranium oxide as a function of O/U atom ratio is presented in Table XII and Fig. 37. The damping of the hyperstoichiometric bars became so high that the decay method was unsuitable, and the determinations were made by the half-width method.

The logarithm of the internal friction of urania increased linearly with an excess of oxygen. That must have been the result of the increased precipitation of U_4O_9. This seems consistent with the results obtained for samples 49-1 and 50-1. The latter, as was explained before, had a larger amount of U_4O_9 than did 49-1, and that must have been the reason for the damping increase noticed in Table XII and Fig. 37.

No plausible explanation was found for the discrepant internal-friction result of the sample with composition $UO_{2.081}$.

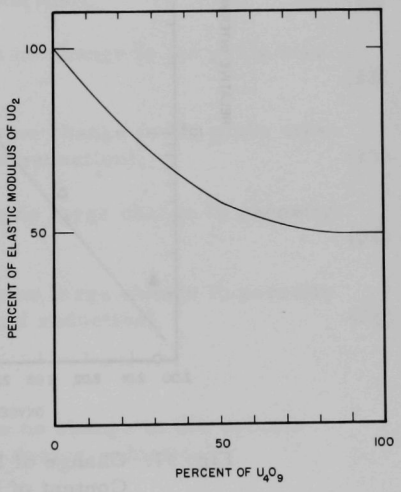

Fig. 36. Hypothetical Variation of Elastic Modulus with Ratio of UO_2 to U_4O_9

TABLE XII. Effect of Oxygen Content on Internal Friction of Urania

Sample	O/U	Q_R^{-1} [a]	Remarks	Sample	O/U	Q_R^{-1} [a]	Remarks
30	2.005	100	Quenched at 450°C	30-R	2.026	550	Oxidized to $UO_{2.084}$ and then reduced in H_2
32	2.005	100	Quenched at 450°C	34-1	2.055	2,725	Quenched at 450°C
34	2.005	100	Quenched at 450°C	49-1	2.073	2,900	Quenched at 800°C
36	2.005	100	Quenched at 450°C	50-1	2.075	7,800	Quenched at 450°C
37	2.005	100	Quenched at 450°C	36-1	2.081	3,225	Quenched at 450°C
49	2.005	100	Quenched at 450°C	37-1	2.107	38,500	Quenched at 450°C
50	2.005	100	Quenched at 450°C				
32-R	2.005	233	Oxidized to $UO_{2.081}$ and then reduced in H_2				

[a] $Q_{RA}^{-1} = \frac{Q_A^{-1}}{Q_I^{-1}} \times 100$,

where Q_{RA}^{-1} is the relative internal friction for a sample with an O/U ratio of A, Q_A^{-1} is the absolute internal friction for a sample with an O/U ratio of A, and Q_I^{-1} is the absolute internal friction for a sample with the initial O/U ratio (2.005).

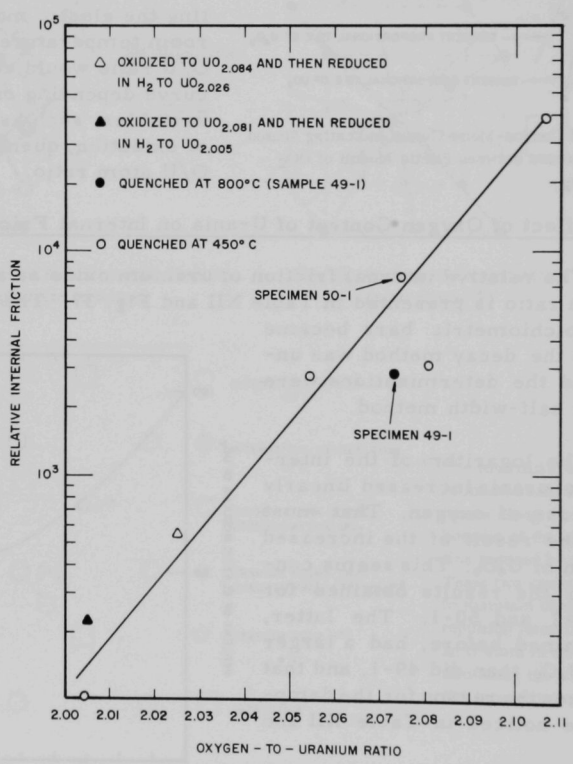

Fig. 37. Change of Internal Friction with Oxygen Content of Urania at Room Temperature

The relative internal friction could be expressed by

$$Q_R^{-1} = Q_{RC}^{-1} + Q_{RG}^{-1} + Q_{RP}^{-1} + Q_{RSP}^{-1}, \quad (17)$$

where Q_R^{-1} is the total relative internal friction, Q_{RC}^{-1} is the relative internal friction due to the cracks, Q_{RG}^{-1} is the relative internal friction due to the grain boundaries, Q_{RP}^{-1} is the relative internal friction due to the porosity, and Q_{RSP}^{-1} is the relative internal friction introduced by the second phase.

The relative internal friction for (a) the initial sample (Q_{Ri}^{-1}), (b) the bar (37-1) after oxidation (Q_{Ro}^{-1}), and (c) the specimen (32-R) after reduction (Q_{Rr}^{-1}) may be expressed as

$$Q_{Ri}^{-1} = Q_{RCi}^{-1} + Q_{RGi}^{-1} + Q_{RPi}^{-1} + Q_{RSPi}^{-1} = 100, \quad (18)$$

$$Q_{Ro}^{-1} = Q_{RCo}^{-1} + Q_{RGo}^{-1} + Q_{RPo}^{-1} + Q_{RSPo}^{-1} = 38{,}500, \quad (19)$$

and

$$Q_{Rr}^{-1} = Q_{RCr}^{-1} + Q_{RGr}^{-1} + Q_{RPr}^{-1} + Q_{RSPr}^{-1} = 233. \quad (20)$$

In these expressions,

$$Q_{RCi}^{-1} = Q_{RSPi}^{-1} = Q_{RSPr}^{-1} = 0 \text{ (because there were no cracks in the initial sample, and no second phase was present in the sample before oxidation or after reduction),} \quad (21)$$

$$Q_{RGi}^{-1} = Q_{RGo}^{-1} \text{ (because there was no change in the grain size during oxidation),} \quad (22)$$

$$Q_{RGi}^{-1} = Q_{RGr}^{-1} \text{ (because there was no change in the grain size after oxidation and reduction),} \quad (23)$$

$$Q_{RPi}^{-1} \sim Q_{RPo}^{-1} \text{ (because there was no large change in porosity during oxidation),} \quad (24)$$

$$Q_{RPi}^{-1} \sim Q_{RPr}^{-1} \text{ (because there was no large change in porosity during oxidation and reduction),} \quad (25)$$

and

$$Q_{RCo}^{-1} \sim Q_{RCr}^{-1} \text{ (because there was no change in the volume percent of cracks during reduction).} \quad (26)$$

Then from Equations (18) and (19) and introducing Equations (21), (22), and (24), we obtain

$$Q_{Ro}^{-1} - Q_{Ri}^{-1} = Q_{RCo}^{-1} + Q_{RSPo}^{-1} = 38{,}400. \tag{27}$$

From Equations (20) and (18) and introducing Equations (21), (23), and (25), we obtain

$$Q_{Rr}^{-1} - Q_{Ri}^{-1} = Q_{RCr}^{-1} = 133. \tag{28}$$

Then from Equations (26), (27), and (28),

$$Q_{Ro}^{-1} - Q_{Rr}^{-1} = Q_{RSPo}^{-1} = 38{,}267, \tag{29}$$

indicating that the main contribution to the internal friction of nonstoichiometric urania is produced by the second phase.

VII. CONCLUSIONS

The elastic modulus of sintered compacts of stoichiometric uranium oxide at room temperature increases with increasing density. When the volume-fraction porosity is less than 0.1, either a linear or an exponential equation can be used to calculate the elastic trait as a function of density. When the volume-fraction porosity becomes greater than 0.1, a linear equation seems to be the most suitable. The linear expression is given by $E = 2233.85(1 - 2.277P)$, and the exponential equation by $E = 2243.56e^{-2.52P}$; where E is the elastic modulus of porous polycrystalline uranium oxide, and P is the volume-fraction porosity. The elastic modulus of stoichiometric, nonporous uranium dioxide at room temperature was found by extrapolation to be 2243.56 ± 22.1 kilobars when the exponential equation was used, and 2233.85 ± 22.05 kilobars when the linear expression was used.

Internal friction of $UO_{2.00}$ decreased sharply as the grain size increased. Other microstructural characteristics, namely, number, size, and position of pores also contribute to this behavior. In nonstoichiometric urania, the presence of a two-solid phase is the pre-eminent factor dictating the damping properties at room temperature.

Young's modulus for nonstoichiometric uranium oxide at room temperature depends mainly on the history of the sample. Varying the oxidation and/or the rate of cooling will produce completely different results.

When studying or specifying the elastic or anelastic trait of nonstoichiometric urania at room temperature, one must characterize the material not only by the oxygen-to-uranium atom ratio, but also by microstructure, particularly the number, location, and quantity of solid phases present and the type of porosity. In the oxidation range studied here, the ratio of UO_{2+x} to U_4O_9 (or U_4O_{9-y}) is advisable to relate properties at room temperature to uranium-oxygen content.

APPENDIX A

Characteristics of the Instruments for the Determination of the Elastic Modulus and Internal Friction

TABLE A-I. Characteristics of Storage Oscilloscope (Cathode-ray Storage Tube)

Type	Tetronix T5640-201
Accelerating voltage	3.5 kV
Deflection-plate sensitivity	
a) Horizontal	17.5 to 19.3 V/cm
b) Vertical	18.5 to 20.5 V/cm
Storage time	Up to 1 hr
Writing rate	Initially 10 μsec/cm
Contrast ratio	2 to 1 minimum
Erase time	Approximately 0.25 sec

TABLE A-II. Characteristics of Differential Amplifier

Type	Tetronix 2A63--Differential
Rejection ratio	50:1
Passband	DC, 300 kc
Sensitivity	1 mV/division to 20 V/division in 14 steps, 1-2-5 sequence. Uncalibrated continuous control from 1 mV/division to 50 V/division.
Accuracy	Within 3%
Phase shift	Nominally less than 1° at 50 kc
Input impedance	1 MΩ, paralleled by approximately 47 pF

TABLE A-III. Characteristics of Time Base

Type	Tetronix 2B67
Calibrated sweep range	1 μsec/division to 5 sec/division in 21 steps, 1-2-5 sequence. Uncalibrated continuous control from 1 μsec/division to 12 sec/division.
Accuracy	3%, with magnifier, 5%
Single sweep	Operates only after manual reset for either triggered or full-running operation
Triggering modes	Internal, external, and line. Trigger coupling may be selected from a.c. slow, a.c. fast, and d.c.; triggering level and polarity are continuously adjustable. Triggering level may be set to provide free-running or automatically triggered sweeps.
Triggering signal	Internal: a signal producing two minor divisions of deflection.
	External: a signal from 0.5 V at d.c. to 2.0 V at 2 Mc. Sweep will trigger on larger signals, but level control limit is ±10 V.
External Signal input	Bandpass: d.c. to about 750 kc. Sensitivity: about 1 V/division.

TABLE A-IV. Characteristics of Vacuum-tube Voltmeter

Type	Hewlett-Packard 400 DR
Voltage range	0.001 to 300 V in 12 ranges
Decibel range	-72 to +52 db, in 12 ranges
Frequency range	10 cps to 4 Mc
Input impedance	10 MΩ shunted by 15 pF on ranges 1.0 to 300 V; 25 pF on ranges 0.001 to 0.3 V.
Amplifier	Output terminals are provided so that the voltmeter can be used to amplify small signals or to enable monitoring of waveforms under test with an oscilloscope. Output voltage is approximately 0.15 V on all ranges with full-scale meter deflection.
Accuracy	±2% of full scale, 20 cps to 1 Mc ±3% of full scale, 20 cps to 2 Mc ±5% of full scale, 10 cps to 4 Mc

TABLE A-V. Characteristics of Audio Oscillator

Type	Hewlett-Packard 201 CR
Frequency range	20 cps to 20 kc
Frequency stability	±2%
Frequency response	±1% db over entire frequency range (reference 1 kc)
Output	3 W max or 42.5 V 600 Ω load
Distortion	Less than 0.5%, 50 cps to 20 kc at 1 W output. Less than 1%, 20 cps to 20 kc at 3 W output.
Attenuator	0-40 db in 10-db steps. Concentric amplitude control varies output continuously from zero to maximum at any attenuator setting.
Internal impedance	Approximately 75 Ω below 5000 cps at 0-db setting of attenuator. Approximately 600 Ω over entire frequency range with output attenuator at 10 db or more.
Hum voltage	Less than 0.03% of rated or attenuated output (amplitude control at maximum)

TABLE A-VI. Characteristics of Frequency Counter

Type	Computer Measurements Company 225A
Frequency range	1 cps to 100 kc
Readout	5 decades
Input impedance	0.5 MΩ, 50-pF shunt
Gate times	100 μsec to 10 sec in 5-decade steps
Accuracy	±1 count ± oscillator accuracy (± trigger level error for period measurement)

TABLE A-VII. Characteristics of Power Amplifier

Type	McIntosh MI-75
Power output	75 W
Frequency response	+ 0 - 0.2 db, 20 cps to 20 kc + 0 - 1 db, 18 cps to 40 kc
Gain control	Accommodate input levels from 0.5 to 30 V
Output impedance	4, 8, 16, 67, 150, and 600 Ω
Output voltage	25, 70.7, 115, and 230 V
Input impedance	High and low. When a low-impedance line input or bridging input is desired, a plug-in input must be used.

TABLE A-VIII. Characteristics of Driver

Type	Astatic Cutting Head M41-500
Input impedance	500 Ω
Maximum input voltage	40 V
Frequency response	Flat

TABLE A-IX. Characteristics of Pickup

Type	Astatic Phonograph Cartridge L-12
Output voltage	4 V
Needle pressure	28.35 g
Frequency range	50-5000 cps
Output impedance	1 MΩ or more.

APPENDIX B

Finishing Operation of Specimens for Elastic and Anelastic Studies

Specimens were finished on lapping wheels with the aid of the stainless-steel jig shown in Fig. B-1. The specimen was placed inside of the device (C) that was resting on a flat surface. Cold-mounting mixture was poured in until the sample was covered. This mounting held the bar and minimized the stresses during the grinding. With the help of the plunger (B), the specimen and the mounting were pushed from the flat side until part of the specimen protruded from the jig. The screws in the jig were tightened against the plunger, and the projecting part of the mounted specimen were ground until a flat surface was obtained. The screws were loosened, and the same process was repeated, but starting from the newly flat surface. When the grinding was near completion, the mounted specimen was removed from the jig. A gauge (A) was put inside of the device and pressed with the plunger against a flat surface. Then the screws were tightened, holding the plunger in the correct position. After the gauge was removed, the mounted sample was replaced and finished. The grinding was started with silicon paper number 80, followed by 120, 240, 400, and 600. These steps produced two flat and parallel surfaces. The specimen was taken from the jig and dismounted with the help of a hot wire. Then the procedure was repeated with the other two faces.

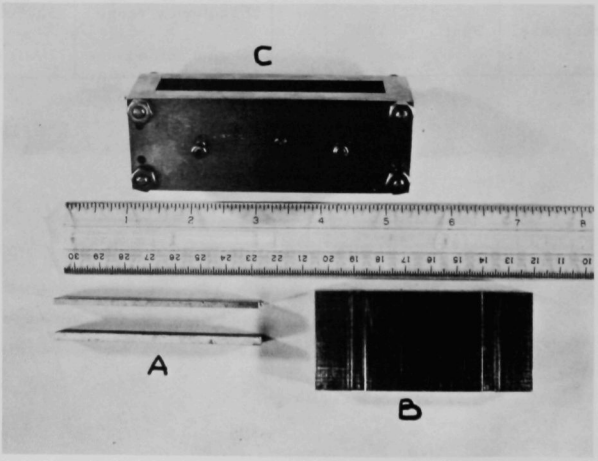

Fig. B-1. Device Employed for Finishing the Bars

APPENDIX C

Calculation of the Elastic Modulus

1. Calculation Formula

The elastic modulus was calculated from the expression

$$E = 0.94645 \times \frac{C \times m \times f_r^2}{D}, \qquad \text{(C-1)}$$

where E is Young's modulus, m is the mass of the specimen, f_r is the resonant frequency of the fundamental mode of flexural vibration, D is the dimension of the cross section perpendicular to the direction of vibration, and C is a factor given by Hasselman's table[8] as a function of the dimension of the cross section parallel to the direction of vibration, the length, and Poisson's ratio (μ).

Lang[62] has reported values of Poisson's ratio varying from 0.291 to 0.306. For the present calculations it has been assumed to be 0.30.

2. Example of Calculation

a. Data

Dimensions of cross section: 0.326 x 0.231 cm

Length, L: 6.799 cm

Mass, m: 5.4280 g

Flatwise resonant frequency:* 2254.2 cps

Edgewise resonant frequency:** 3166 cps

b. Flatwise Elastic Modulus (E_f)

To enter Hasselman's table, the ratio of D to L must be calculated. In this example,

$$\frac{D}{L} = \frac{0.231}{6.799} = 0.0340.$$

---

*This is the resonant frequency when the vibration is perpendicular to the longer side of the cross section.

**This is the resonant frequency when the vibration is perpendicular to the shorter side of the cross section.

From this value and assuming $\mu = 0.30$ from Hasselman's table, we obtain

$$C = 25654.5.$$

Then,

$$E_f = 0.94645 \times \frac{25654.5 \times 5.4280 \times (2254.2)^2}{0.326}$$

$$= 2054.03 \times 10^9 \text{ dynes/cm}^2$$

$$= 2054.03 \text{ kilobars.}$$

c. Edgewise Elastic Modulus (E_e)

Similarly,

$$\frac{D}{L} = \frac{0.326}{6.799} = 0.0479.$$

Then

$$C = 9249.07.$$

Therefore,

$$E_e = 0.94645 \times \frac{9249.07 \times 5.4280 \times (3166)^2}{0.231}$$

$$= 2061.74 \times 10^9 \text{ dynes/cm}^2$$

$$= 2061.74 \text{ kilobars.}$$

APPENDIX D

Calculation of the Internal Friction

1. Example of Calculation of the Internal Friction by the Decay Method

a. Data

(A_0, A_1, and Δt were obtained from Fig. D-1.)

$2A_0 = 260$ mV;

$2A_1 = 130$ mV;

$\Delta t = 0.2$ sec;

$f_r = 2270$ cps.

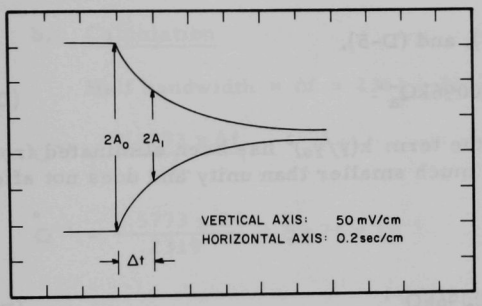

Fig. D-1

Decay of Amplitude of Vibration Traced from Storage Oscilloscope

b. Calculation

$$Q^{-1} = \frac{\ell n \frac{2A_0}{2A_1}}{\pi \times f_r \times \Delta t}$$

$$= \frac{\ell n\ 0.693}{3.14 \times 2270 \times 0.2} = 4.86 \times 10^{-4}. \qquad \text{(D-1)}$$

2. Calculation of Q_s^{-1} Employing the Equation Given by Wachtman and Tefft[46]

$$Q_m^{-1} = \frac{Q_s^{-1} + kQ_a^{-1}(y/y_0)^2}{1 + k(y/y_0)^2} \qquad \text{(D-2)}$$

where Q_m^{-1} is the internal friction actually obtained from a measurement, Q_s^{-1} is the absolute internal friction of the sample, Q_a^{-1} is the internal friction of the apparatus, k is a constant for a given specimen and suspension,

$$(y/y_0)^2 = \frac{1.018[\cosh(4.730x/\ell) + \cos(4.730x/\ell)] - [\sinh(4.730x/\ell) - \sin(4.730x/\ell)]}{2.036},$$

x is the distance of suspension from end, and ℓ is the length of the specimen. Values of $(y/y_0)^2$ have been tabulated by Wachtman and Tefft.[46]

a. Data

$$Q_m^{-1} = 1.80 \times 10^{-4} \text{ when } x/\ell = 0.200; \quad \text{(D-3)}$$

$$Q_m^{-1} = 7.79 \times 10^{-4} \text{ when } x/\ell = 0.150; \quad \text{(D-4)}$$

$$(y/y_0)^2 = 0.0096 \text{ when } x/\ell = 0.200; \quad \text{(D-5)}$$

$$(y/y_0)^2 = 0.0973 \text{ when } x/\ell = 0.150. \quad \text{(D-6)}$$

b. Calculation

From (D-2), (D-3), and (D-5),

$$1.80 \times 10^{-4} = Q_s^{-1} + 0.0096kQ_a^{-1}. \quad \text{(D-7)}$$

To simplify the calculations, the term $k(y/y_0)^2$ has been eliminated from Equation (D-2). This term is much smaller than unity and does not affect, practically, the value of Q_m^{-1}.

Then,

$$Q_s^{-1} = 1.80 \times 10^{-4} - 0.0096kQ_a^{-1}. \quad \text{(D-8)}$$

Substituting (D-4), (D-6), and (D-8), in (D-2), we obtain

$$7.79 \times 10^{-4} = (1.80 \times 10^{-4} - 0.0096kQ_a^{-1}) + 0.0973kQ_a^{-1}, \quad \text{(D-9)}$$

or

$$kQ_a^{-1} = 0.683 \times 10^{-2}. \quad \text{(D-10)}$$

Substituting (D-10) in (D-7), we obtain

$$Q_s^{-1} = 1.80 \times 10^{-4} - [(0.683 \times 10^{-2})(0.96 \times 10^{-2})], \quad \text{(D-11)}$$

or

$$Q_s^{-1} = 1.15 \times 10^{-4}. \quad \text{(D-12)}$$

3. Calculation of the Internal Friction by the Half-bandwidth Method

a. Data

Background amplitude (A_B) = 15 mV;

Amplitude at resonance frequency (A_R) = 61 mV;

Resonance frequency (f_r) = 2319 cps;

True amplitude (A_T) = $A_R - A_B$ = 46 mV;

Half-bandwith amplitude (A_{HB}) = $\frac{A_T}{2} + A_B$

= 23 + 15 = 38 mV;

Frequencies at A_{HB} = 2307 and 2331 cps.

b. Calculation

Half bandwidth = Δf = 2331 - 2307 = 24 cps;

$$Q^{-1} = \frac{0.5773 \times \Delta f}{f_r}; \qquad \text{(D-13)}$$

$$Q^{-1} = \frac{0.5773 \times 24}{2319} = 59.74 \times 10^{-4}. \qquad \text{(D-14)}$$

APPENDIX E

Determination of Oxygen-to-Uranium Atom Ratio

1. Determination of an Unknown Oxygen-to-Uranium Ratio

a. A Coors-alumina crucible was heated at 800°C in air and placed in a desiccator.

b. The material to be analyzed was crushed and kept overnight in a desiccator to eliminate the moisture.

c. The crucible was weighed empty and containing the material (about 5 g).

d. The container and powder were introduced in a furnace, and the temperature was raised to 800°C.

e. The material was removed from the furnace, left in air for 5 min, and then placed into a desiccator until completely cool.

f. The weight was determined.

g. Steps 4, 5, and 6 were repeated until there was no further change in weight, indicating that all the material had been oxidized to $UO_{2.667}$.

h. The O/U ratio was calculated from

$$\frac{O}{U} = \left[17.546\left(\frac{W_B}{W_A}\right)\right] - 14.879, \qquad \text{(E-1)}$$

where W_B is the weight of the material before oxidation, and W_A is the weight of the material after oxidation. Expression (E-1) is derived as follows:

The number of moles before and after oxidation is given by

$$n_B = \frac{W_B}{\text{Mol Wt } UO_{X_u}} = \frac{W_B}{\text{Mol Wt U} + X_u \text{ Mol Wt O}} = \frac{W_B}{238.07 + 16X_u},$$

and

$$n_A = \frac{W_A}{\text{Mol Wt } UO_{2.667}} = \frac{W_A}{\text{Mol Wt U} + 2.667 \text{ Mol Wt O}} = \frac{W_A}{280.742}.$$

Since

$$n_B = n_A,$$

it follows that

$$\frac{W_B}{238.07 + 16X_u} = \frac{W_A}{280.742}.$$

Then,

$$16X_u = \left[280.742\left(\frac{W_B}{W_A}\right)\right] - 238.07,$$

or

$$X_u = \left[\frac{280.742}{16}\left(\frac{W_B}{W_A}\right)\right] - \frac{238.07}{16}$$

$$= \left[17.546\left(\frac{W_B}{W_A}\right)\right] - 14.879.$$

2. Determination of the Oxygen-to-Uranium Ratio When the Initial Ratio Is Known

The ratio is obtained from

$$X_u = \left[(14.879 + X_N)\left(\frac{W_A}{W_B}\right)\right] - 14.879, \qquad \text{(E-2)}$$

where

W_A = final weight,

and

W_B = initial weight.

Expression (E-2) is derived as follows:

$$n_B = \frac{W_B}{\text{Mol Wt } UO_{X_N}} = \frac{W_B}{\text{Mol Wt U} + X_N \text{ Mol Wt O}} = \frac{W_B}{238.07 + 16X_N},$$

and

$$n_A = \frac{W_A}{\text{Mol Wt } UO_{X_u}} = \frac{W_A}{\text{Mol Wt U} + X_u \text{ Mol Wt O}} = \frac{W_A}{238.07 + 16X_u}.$$

Since

$$n_B = n_A,$$

it follows that

$$\frac{W_B}{238.07 + 16X_N} = \frac{W_A}{238.07 + 16X_u}$$

or

$$\frac{238.07 + 16X_u}{238.07 + 16X_N} = \frac{W_A}{W_B}.$$

Therefore

$$16X_u = \left[238.07 + 16X_N\left(\frac{W_A}{W_B}\right)\right] - 238.07,$$

or

$$X_u = \left[\left(\frac{238.07}{16} + \frac{16X_N}{16}\right)\left(\frac{W_A}{W_B}\right)\right] - \frac{238.07}{16}$$

$$= \left[(14.879 + X_N)\left(\frac{W_A}{W_B}\right)\right] - 14.879.$$

ACKNOWLEDGMENTS

The authors are indebted to Joseph H. Handwerk, Group Leader of Ceramic Engineering, for making facilities available. The members of the Ceramic Engineering Group are thanked for the discussions that helped to improve this work. Dr. Leon M. Atlas is thanked for his explanation in the use of the computer technique, and Dr. Melvin H. Mueller for his suggestions in the interpretation of X-ray diffraction films. Particular thanks are extended to Gabriel M. Dragel for helping in the preparation of specimens, to Roy A. Conner, Jr., for encapsulating the samples for the oxidation studies, and to David E. White and Joseph T. Dusek for their practical suggestions.

REFERENCES

1. Stokes, R. J., "Correlation of Mechanical Properties with Microstructure," Microstructure of Ceramic Materials, United States Department of Commerce, National Bureau of Standards, Miscellaneous Publication 257 (1964).

2. Chang, R., "The Elastic and Anelastic Properties of Refractory Materials for High Temperature Applications," Mechanical Properties of Engineering Ceramics, W. W. Kriegel and H. Palmour III, Interscience Publishers, New York, London (1961).

3. Belle, J., Uranium Dioxide: Properties and Nuclear Applications, U. S. Government Printing Office, Washington 25, D. C. (1961).

4. Pickett, G., Equations for Computing Elastic Constants from Flexural and Torsional Resonant Frequencies of Vibration of Prisms and Cylinders, Am. Soc. Testing Mater. Proc. 45, 846-865 (1945).

5. Spinner, S., Reichard, T. W., and Tefft, W. E., Comparison of Experimental and Theoretical Relations Between Young's Modulus and the Flexural and Longitudinal Frequencies of Uniform Bars, J. Res. Natl. Bur. Std. (U. S.) 64A, 147-155 (1960).

6. Spinner, S., and Tefft, W. E., A Method for Determining Mechanical Resonance Frequencies and for Calculating Elastic Moduli from These Frequencies, Am. Soc. Testing Mater. Proc. 61, 1221-1238 (1961).

7. Lakin, J. R., Determination of the Elastic Constants of Refractories by a Dynamic Method, Trans. Brit. Ceram. Soc. 56, 1-7 (1957).

8. Hasselman, D. P. H., Tables for the Computation of the Shear Modulus and Young's Modulus of Elasticity from the Resonant Frequencies of Rectangular Prisms, Applied Research Branch, Research and Development Division, The Carborundum Company, Niagara Falls, New York (1961).

9. Spinner, S., and Valore, R. C., Jr., Comparison of Theoretical and Empirical Relations Between the Shear Modulus and Torsional Resonance Frequencies for Bars of Rectangular Cross Section, J. Res. Natl. Bur. Std. (U. S.) 60(5), 459-464 (1958).

10. Tefft, W. E., and Spinner, S., Torsional Resonance Vibrations of Uniform Bars of Square Cross Section, J. Res. Natl. Bur. Std. (U. S.) 65A(3), 167-171 (1961).

11. Mason, W. P., Physical Acoustics and the Properties of Solids, D. Van Nostrand Company (1958).

12. Kolsky, H., Stress Waves in Solids, Clarendon Press (1953).

13. Zener, C. M., Elasticity and Anelasticity of Metals, The University of Chicago Press (1948).

14. Dew, R. J., Jr., Damping Capacity Measurements on Refractory Oxides under Varying Stress and Temperature Conditions, ScD thesis, MIT (1950).

15. Chang, L. C., and Gensamer, M., Internal Friction of Iron and Molybdenum at Low Temperature, Acta Met. 1(9), 483-486 (1953).

16. Ault, N. N., and Ueltz, H. F. G., Sonic Analysis for Solid Bodies, J. Am. Ceram. Soc. 36(6), 199-203 (1953).

17. Balamuth, L., A New Method for Measuring Elastic Moduli and the Variation with Temperature of the Young's Modulus of Rocksalt Between 78°K and 273°K, Phys. Rev. 45(5), 715-720 (1953).

18. Read, T., Internal Friction of Single Metal Crystals, Phys. Rev. 58(8), 371-380 (1940).

19. Marx, J., Use of Piezoelectric Gauge for Internal Friction Measurements, Rev. Sci. Instr. 22(7), 503-509 (1951).

20. Bancroft, D., and Jacobs, R., An Electrostatic Method of Measuring Elastic Constants, Rev. Sci. Instr. 9(9), 279-281 (1938).

21. Dickson, E. W., and Strauch, H., Apparatus for Measurement of the Internal Friction of Metals at Kilocycle Frequencies, J. Sci. Instr. 36(10), 425-428 (1959).

22. Fine, M. E., Apparatus for Precise Determination of Dynamic Young's Modulus and Internal Friction at Elevated Temperatures, Rev. Sci. Instr. 28(8), 643-645 (1958).

23. Sneed, R. J., Fink, E. L., and Abrams, M. C., Anelastic Behavior of Tantalum and Columbium, ASD-TDR-62-323 (1963).

24. Förster, F., A New Method for the Determination of the Modulus of Elasticity and Damping, Z. Metallkunde 29(4), 116-123 (1937).

25. Steierman, B. L., Wu, J. C. C., and McCormick, J. M., Note on Ultrasonic Absorption of Glass at Elevated Temperatures, J. Am. Ceram. Soc. 38(6), 211-213 (1955).

26. Krause, J. T., Differential Path Method for Measuring Ultrasonic Velocities in Glasses at High Temperatures, J. Acoust. Soc. Am. 35(1), 1-4 (1963).

27. Strakna, R. E., and Savage, H. T., Ultrasonic Relaxation Loss in SiO_2, GeO_2, B_2O_3, and As_2O_3 Glasses, J. Appl. Phys. 35(5), 1445-1450 (1964).

28. Anderson, O. L., and Bömmel, H. E., Ultrasonic Absorption in Fused Silica at Low Temperatures and High Frequencies, J. Am. Ceram. Soc. 38(4), 125-131 (1955).

29. Keler, E. K., Kozlovskaya, E. I., and Nosikov, O. V., Determination of the Elastic Properties of Glass and Fine Ceramics by the Ultrasonic Impulse Method, Glass and Ceramics (Steklo i Keramika) 13(5), 211-218 (1956).

30. Fraser, D. B., Anelastic Effects of Alkali Ions in Crystalline Quartz, J. Appl. Phys. 35(10), 2913-2918 (1964).

31. Carnevale, E. H., Lynnworth, L. C., and Larson, G. S., Ultrasonic Measurement of Elastic Moduli at Elevated Temperatures Using Momentary Contacts, J. Acoust. Soc. Am. 36(9), 1678-1684 (1964).

32. Ke, T. S., Experimental Evidence of the Viscous Behavior of Grain Boundaries in Metals, Phys. Rev. 71(8), 533-546 (1947).

33. Fitzgerald, J. V., Anelasticity of Glass: I. Introduction, J. Am. Ceram. Soc. 34(10), 314-319 (1951).

34. Rindone, G. E., Glass Research by Internal Friction Measurements, Mineral Industries 31(4), 1-6 (1962).

35. Kofstad, P., Butera, R. A., and Craig, R. S., Apparatus for Continuous Recording of Internal Friction, Rev. Sci. Instr. 33(8), 850-853 (1962).

36. Chang, R., High Temperature Creep and Anelastic Phenomena in Polycrystalline Refractory Oxides, J. Nucl. Materials 1(2), 174-181 (1959).

37. Fraser, D. B., and LeCraw, R. C., Novel Method of Measuring Elastic and Anelastic Properties of Solids, Rev. Sci. Instr. 35(9), 1113-1115 (1964).

38. Roberts, M. H., and Nortcliffe, J., Measurement of Young's Modulus at High Temperatures, J. Iron and Steel Institute 159(11), 345-348 (1947).

39. Baskin, Y., Harada, Y., and Handwerk, J. H., Some Physical Properties of Thoria Reinforced by Metal Fibers, J. Am. Ceram. Soc. 43(9), 489-492 (1960).

40. Wachtman, J. B., Jr., and Maxwell, L. H., Factors Controlling Resistance to Deformation and Mechanical Failure in Polycrystalline (Glass-free) Ceramics, WADC 57-526 (1957).

41. Brown, H. L., and Armstrong, P. E., Young's Modulus Measurements Above 2000°C, Rev. Sci. Instr. 34(6), 636-639 (1963).

42. Marlowe, M. O., and Wilder, D. R., Elasticity and Internal Friction of Polycrystalline Yttrium Oxide, J. Am. Ceram. Soc. 48(5), 227-233 (1965).

43. Spinner, S., Elastic Moduli of Glasses at Elevated Temperatures by a Dynamic Method, J. Am. Ceram. Soc. 39(3), 113-118 (1956).

44. Willmore, T. A., Degenkolb, R. S., Herron, R. H., and Allen, A. W., Application of Sonic Moduli of Elasticity and Rigidity to Testing of Heavy Refractories, J. Am. Ceram. Soc. 37(10), 445-457 (1954).

45. Wachtman, J. B., Jr., Tefft, W. E., and Lam, D. G., Jr., Elastic Constants of Rutile, J. Res. Natl. Bur. Std. (U. S.) 66A(6), 465-472 (1962).

46. Wachtman, J. B., Jr., and Tefft, W. E., Effect of Suspension Position on Apparent Values of Internal Friction Determined by Förster's Method, Rev. Sci. Instr. 29(6), 517-520 (1958).

47. Förster, F., and Breitfeld, H., Ein Gerät zur Unmittelbaren Dämpfungsanzeige, Z. Metallkunde 30(9), 343-345 (1938).

48. Pattison, J. R., An Apparatus for the Accurate Measurement of Internal Friction, Rev. Sci. Instr. 25(5), 490-496 (1954).

49. Thompson, D. O., and Holmes, D. K., Effects of Neutron Irradiation Upon the Young's Modulus and Internal Friction of Copper Single Crystals, J. Appl. Phys. 27(7), 713-723 (1956).

50. Brown, R. M., Bickelhaupt, R. E., and Allen, A. W., High Temperature Thermal Properties of Ceramic-Metal Combinations, Fifth Summary Report, Bendix Products Aerospace Division, The Bendix Corporation (1963).

51. Wŏmack, R. E., Modulus of Elasticity Equipment for Hot Cell Application, UCRL-7173 (1963).

52. Sosin, A., Bienvenue, L., and Schlein, H., Internal Friction Measurements, Rev. Sci. Instr. 29(7), 657-658 (1958).

53. Harlow, R. G., Hinton, T., and Rider, J. G., A Frequency Modulation Technique for the Measurement on Internal Friction, J. Sci. Instr. 39(12), 598-599 (1962).

54. Detwiler, D. P., and Holden, S. J., Precision Measurement of Internal Friction in Non-metallic Materials, ARL 64-160 (1964).

55. Smith, G. M., and Berns, H. D., Frequency-Phase Method for Measuring Material Damping, Materials Research and Standard 4(5), 225-227 (1964).

56. Lambertson, W. A., and Handwerk, J. H., The Fabrication and Physical Properties of Urania Bodies, ANL-5053 (1956).

57. Bowers, D. J., Hedden, W. A., Snyder, J. M., and Duckworth, W. H., Effect of Ceramic or Metal Additives in High-UO_2 Bodies, BMI-1117 (1956).

58. Johnson, J. R., "Ceramic Fuel Materials for Nuclear Reactors," Selected Papers from First Nuclear Engineering Congress, Vol. I, Pergamon Press (1957).

59. Belle, J., and Lustman, B., Properties of Uranium Dioxide, Fuel Elements Conference, Book 2, TID-7546 (1958).

60. Scott, R., Hall, A. R., and Williams, J., The Plastic Deformation of Uranium Oxides Above 800°C, J. Nucl. Materials 1(1), 39-48 (1959).

61. Wachtman, J. B., Jr., Tefft, W. E., Lam, D. G., Jr., and Stinchfield, R. P., Factors Controlling Resistance to Deformation and Mechanical Failure in Polycrystalline (Glass-free) Ceramics, WADC-TR-59-278 (1959).

62. Lang, S. M., Properties of High Temperature Ceramic and Cermets. Elasticity and Density at Room Temperature, Natl. Bur. Std. (U.S.), Monograph 6 (1960).

63. Wachtman, J. B., Jr., Wheat, M. L., Anderson, H. J., and Bates, J. L., Elastic Constants of Single Crystal UO_2 at 25°C, J. Nucl. Materials 16(1), 39-41 (1965).

64. Coble, R. L., and Kingery, W. D., Effect of Porosity on Physical Properties of Sintered Alumina, J. Am. Ceram. Soc. 39(11), 377-385 (1956).

65. Mackenzie, J. K., Elastic Constants of a Solid Containing Spherical Holes, Proc. Phys. Soc. (London) 63B(1), 2-11 (1950).

66. Fenstermacher, J. E., and Hummel, F. A., Apparent Relation Between Elastic Modulus and Transverse Modulus of Rupture, J. Am. Ceram. Soc. 44(6), 297 (1961).

67. Spriggs, R. M., Expression for Effect of Porosity on Elastic Modulus of Polycrystalline Refractory Materials, Particularly Al_2O_3, J. Am. Ceram. Soc. 44(12), 628-629 (1961).

68. Spriggs, R. M., and Brissette, L. A., Expression for Shear Modulus and Poisson's Ratio of Porous Refractory Oxides, J. Am. Ceram. Soc. 45(4), 198-199 (1962).

69. Spriggs, R. M., Effect of Open and Closed Pores on Elastic Moduli of Polycrystalline Alumina, J. Am. Ceram. Soc. 45(9), 454 (1962).

70. Knudsen, F. P., Effect of Porosity on Young's Modulus of Alumina, J. Am. Ceram. Soc. 45(2), 94-95 (1962).

71. Hasselman, D. P. H., On the Porosity Dependence of the Elastic Moduli of Polycrystalline Refractory Materials, J. Am. Ceram. Soc. 45(9), 452-453 (1962).

72. Hashin, Z., Elastic Moduli of Heterogeneous Materials, J. Appl. Mech. 29(1), 143-150 (1962).

73. Piatasik, R. S., and Hasselman, D. P. H., Effect of Open and Closed Pores on Young's Modulus of Polycrystalline Ceramics, J. Am. Ceram. Soc. 47(1), 50-51 (1964).

74. Paul, B., Prediction of Elastic Constants of Multiphase Materials, Transactions AIME 218(1), 36-41 (1960).

75. Hasselman, D. P. H., Experimental and Calculated Young's Moduli of Zirconium Carbide Containing a Dispersed Phase of Graphite, J. Am. Ceram. Soc. 46(2), 103 (1963).

76. Hasselman, D. P. H., Relation Between Effects of Porosity on Strength and on Young's Modulus of Elasticity of Polycrystalline Materials, J. Am. Ceram. Soc. 46(11), 564-565 (1963).

77. Spinner, S., Knudsen, F. P., and Stone, L., Elastic Constant-Porosity Relations for Polycrystalline Thoria, J. Res. Natl. Bur. Std. (U.S.) 67C(1), 39-46 (1963).

78. Dewey, J. M., The Elastic Properties of Materials Loaded with Non-rigid Fillers, J. Appl. Phys. 18(6), 578-581 (1947).

79. Kerner, E. H., The Elastic and the Thermoelastic Properties of Composite Media, Proc. Phys. Soc. (London) 69B, 808-813 (1956).

80. Atlas, L. M., Studies of the Brittle Behavior of Ceramic Materials, Task 15, ASD-TR 61-628 (1963).

81. Hanna, R., Elastic Moduli of Polycrystalline Magnesia Alumina Spinel, J. Am. Ceram. Soc. 46(2), 106 (1963).

82. Hanna, R., and Crandall, W. B., The Young's Modulus and Internal Friction of Polycrystalline MgO at Room Temperature, AROD-2891.1 (1961).

83. Hanna, R., and Crandall, W. B., Dissipation of Energy by the Grain Boundaries, AD 274956 (1962).

84. Southgate, P. D., Studies of the Brittle Behavior of Ceramic Materials, Task 5, ASD-TR 61-628 (1963).

85. Astbury, N. F., and Davis, W. R., Internal Friction in Ceramics, Trans. Brit. Ceram. Soc. 63(1), 1-18 (1964).

86. Marlowe, M. O., and Wilder, D. R., Elasticity and Internal Friction Through the Kilocycle Range: Review and Annotated Bibliography, IS-925 (1964).

87. Wachtman, J. B., and Lam, D. G., Jr., Young's Modulus of Various Refractory Materials as a Function of Temperature, J. Am. Ceram. Soc. 42(5), 254-260 (1959).

88. Spinner, S., and Cleek, G. W., Temperature Dependence of Young's Modulus of Vitreous Germania and Silica, J. Appl. Phys. 31(8), 1407-1410 (1960).

89. Roberts, A. L., Elasticity-Temperature Relationship in Refractories, Trans. Brit. Ceram. Soc. 53, 724-730 (1954).

90. Wachtman, J. B., Jr., Mechanical and Electrical Relaxation in ThO_2 Containing CaO, Phys. Rev. 131(2), 517-527 (1963).

91. Wachtman, J. B., Jr., and Doyle, L. R., Internal Friction in Rutile Containing Point Defects, Phys. Rev. 135A(6), 276-286 (1964).

92. Armstrong, W. M., and Irvine, W. R., Creep Deformation of Non-stoichiometric Uranium Dioxide, J. Nucl. Materials 9(2), 121-127 (1963).

93. Kingery, W. D., Thermal Conductivity: XIV, Conductivity of Multi-component Systems, J. Am. Ceram. Soc. 42 (12), 617-627 (1959).

94. Nichols, R. W., Ceramic Fuels-Properties and Technology, Nucl. Eng. 3(9), 327-333 (1958).

95. Ross, A. M., The Dependence of the Thermal Conductivity of Uranium Dioxide on Density, Microstructure, Stoichiometry, and Thermal Neutron Irradiation, CRFD-817 (1960).

96. Schaner, B. E., Metallographic Determination of the UO_2-U_4O_9 Phase Diagram, J. Nucl. Materials 2(2), 110-120 (1960).

97a. Hilliard, J. E., Estimating Grain Size by the Intercept Method, Metal Progr. 85(5), 99-100 (1964).

97b. Standard Methods for Estimating the Average Grain Size of Metals, ASTM E-112-63, Book of ASTM Standards, Part 1, pp. 587-601 (1965).

98. Knudsen, F. P., Dependence of Mechanical Strength of Brittle Polycrystalline Specimens on Porosity and Grain Size, J. Am. Ceram. Soc. 42(8), 376-387 (1959).

99. Siegel, S., Argonne National Laboratory, personal communication.

100. Grønvold, F., High Temperature X-ray Study of Uranium Oxides in the UO_2-U_3O_8 Region, J. Inorganic Nucl. Chem. 1(6), 357-370 (1955).

101. Perio, P., Oxidation of Uranic Oxide at Low Temperatures, Bull. Soc. Chim. France 20, 256-263 (1953).

102. Blackburn, P. E., Oxygen Dissociation Pressures Over Uranium Oxides, J. Phys. Chem. 62(8), 897-902 (1958).

103. Physical Properties of UO_2 Single Crystals, Quarterly No. 10, EURAEC-1254 (Mar 1-June 30, 1964).

104. Tuxworth, R. H., and Evans, W., Habit Planes for U_4O_9 Precipitation in Uranium Dioxide, J. Nucl. Materials 1(3), 302-303 (1959).

105. Willis, B. T. M., Position of the Oxygen Atoms in $UO_{2.13}$, Nature (2), 755-56 (1963).

106. Willis, B. T. M., Structures of UO_2, UO_{2+x} and U_4O_9 by Neutron Diffraction, Le Journal de Physique 25(5), 431-439 (1964).

107. Hayden, A. W., Moffatt, W. G., and Wulff, J., The Structure and Properties of Materials, Vol. III, John Wiley & Sons, Inc. (1965).